





Ecosystem state shifts during long-term development of an Amazonian peatland

Graeme T. Swindles¹  | Paul J. Morris¹  | Bronwen Whitney²  | Jennifer M. Galloway³ | Mariusz Gałka⁴ | Angela Gallego-Sala⁵ | Andrew L. Macumber⁶ | Donal Mullan⁶ | Mark W. Smith¹  | Matthew J. Amesbury⁵ | Thomas P. Roland⁵ | Hamed Sanei³ | R. Timothy Patterson⁷ | Nicole Sanderson⁵ | Lauren Parry⁸ | Dan J. Charman⁵ | Omar Lopez⁹ | Elvis Valderamma¹⁰ | Elizabeth J. Watson¹ | Ruza F. Ivanovic¹¹ | Paul J. Valdes¹² | T. Edward Turner¹ | Outi Lähteenoja¹³

¹School of Geography, University of Leeds, Leeds, UK

²Department of Geography and Environmental Science, Northumbria University, Newcastle upon Tyne, UK

³Geological Survey of Canada / Commission géologique du Canada, Calgary, Canada & Department of Geoscience, University of Calgary, Calgary, AB, Canada

⁴Department of Biogeography and Palaeoecology, Adam Mickiewicz University, Poznań, Poland

⁵Geography, College of Life and Environmental Sciences, University of Exeter, Exeter, UK

⁶School of Natural and Built Environment, Queen's University Belfast, Belfast, UK

⁷Ottawa-Carleton Geoscience Center and Department of Earth Sciences, Carleton University, Ottawa, ON, Canada

⁸School of Interdisciplinary Studies, University of Glasgow, Glasgow, UK

⁹Panama Instituto de Investigaciones Científicas y Servicios de Alta Tecnología, Panamá & Smithsonian Tropical Research Institute, Panama City, Panama

¹⁰Facultad de Biología, Universidad Nacional de la Amazonia Peruana, Pevas 5ta cdra, Iquitos, Peru

¹¹School of Earth and Environment, University of Leeds, Leeds, UK

¹²School of Geographical Sciences, University of Bristol, Bristol, UK

¹³School of Life Sciences, Arizona State University, Tempe, AZ, USA

Correspondence

Graeme T. Swindles, School of Geography, University of Leeds, Leeds, UK.
Email: g.t.swindles@leeds.ac.uk

Funding information

Natural Environment Research Council, Grant/Award Number: NE/I012915/1, NE/K008536/1; Royal Society, Grant/Award Number: 481831

Abstract

The most carbon (C)-dense ecosystems of Amazonia are areas characterized by the presence of peatlands. However, Amazonian peatland ecosystems are poorly understood and are threatened by human activities. Here, we present an investigation into long-term ecohydrological controls on C accumulation in an Amazonian peat dome. This site is the oldest peatland yet discovered in Amazonia (peat initiation ca. 8.9 ka BP), and developed in three stages: (i) peat initiated in an abandoned river channel with open water and aquatic plants; (ii) inundated forest swamp; and (iii) raised peat dome (since ca. 3.9 ka BP). Local burning occurred at least three times in the past 4,500 years. Two phases of particularly rapid C accumulation (ca. 6.6–6.1 and ca. 4.9–3.9 ka BP), potentially resulting from increased net primary productivity, were seemingly driven by drier conditions associated with widespread drought events. The association of drought phases with major ecosystem state

This is an open access article under the terms of the Creative Commons Attribution License, which permits use, distribution and reproduction in any medium, provided the original work is properly cited.

© 2017 The Authors. *Global Change Biology* Published by John Wiley & Sons Ltd

shifts (open water wetland–forest swamp–peat dome) suggests a potential climatic control on the developmental trajectory of this tropical peatland. A third drought phase centred on ca. 1.8–1.1 ka BP led to markedly reduced C accumulation and potentially a hiatus during the peat dome stage. Our results suggest that future droughts may lead to phases of rapid C accumulation in some inundated tropical peat swamps, although this can lead ultimately to a shift to ombrotrophy and a subsequent return to slower C accumulation. Conversely, in ombrotrophic peat domes, droughts may lead to reduced C accumulation or even net loss of peat. Increased surface wetness at our site in recent decades may reflect a shift towards a wetter climate in western Amazonia. Amazonian peatlands represent important carbon stores and habitats, and are important archives of past climatic and ecological information. They should form key foci for conservation efforts.

KEYWORDS

Amazon rainforest, carbon accumulation, climate, Holocene, palaeoecology, peat, Peru, swamp, tropical peatland

1 | INTRODUCTION

Tropical peatlands are found in Southeast Asia, Central Africa, and Central and South America. They represent globally important terrestrial carbon (C) stores and ecosystems (Page, Rieley, & Banks, 2011) and contain at least 87 Pg (billion tonnes) of C (Moore et al., 2013; Page et al., 2011), similar to the amount stored in the living above-ground biomass of the entire Amazon rainforest (93 ± 23 Pg C—Fauset et al., 2015; Malhi et al., 2006). There is much concern over the future of tropical peatlands because large areas in Southeast Asia have been severely damaged by burning, logging, and conversion to agriculture (Hooijer et al., 2010; Page et al., 2011). In particular, ditch draining of tropical peatlands to convert them to agricultural use can lead to a rapid destabilization of their C stores (Baird et al., 2017). Tropical peatlands are under threat from growing resource exploitation and agricultural expansion in developing nations, and their fate under warmer future climates is unknown.

The Pastaza-Marañón foreland basin (PMFB), NW Peru, contains the most C-dense landscape in Amazonia owing to an abundance of peatlands (e.g., Draper et al., 2014), including nutrient-poor ombrotrophic peat domes and river-influenced minerotrophic peat swamps (Lähteenoja & Page, 2011). It has been estimated that peatlands of the PMFB account for 3.5% of the global tropical peatland C stock, cover $35,600 \pm 2,133$ km², and contain 3.14 (0.44–8.15) Pg C (Draper et al., 2014). One peatland type in particular—pole forest peatland—has been identified as the most C-dense ecosystem type in the Amazon Basin ($1,391 \pm 710$ Mg C/ha) (Draper et al., 2014).

Although much is known about the C dynamics of Amazonian vegetation, including the finding that its ability to store C is diminishing (Brienen et al., 2015), little is known about how Amazonian peatlands developed, including their ecohydrological dynamics through time, C accumulation, and their response to climatic changes. Potential threats to these intact peatlands include hydroelectricity (river

damming) projects, road and railway construction, ore, gas, and oil exploration, logging and clearance of land, and drainage for agriculture—in particular oil palm plantations (Roucoux et al., 2017). Over-exploitation of the fruit of the aguaje palm (*Mauritia flexuosa*—commonly found in wetlands) through tree felling is also of increasing concern (Kahn & Mejia, 1990).

Previous research in the PMFB has included preliminary determinations of peat C content, physical properties, and geochemistry (Lähteenoja & Page, 2011; Lähteenoja, Ruokolainen, Schulman, & Alvarez, 2009; Lähteenoja, Ruokolainen, Schulman, & Oinonen, 2009; Lähteenoja et al., 2012), remote sensing of peatland ecosystems (Draper et al., 2014), and palynological studies (Kelly et al., 2017; Roucoux et al., 2013). There have also been studies of the ecology and palaeoecology of testate amoebae (Reczuga, Swindles, Grewling, & Lamentowicz, 2015; Swindles et al., 2014; Swindles, Lamentowicz, Reczuga, & Galloway, 2016; Swindles, Morris et al., 2016). Watson, Swindles, Savov, and Bacon (2015) reported the presence of microscopic tephra (volcanic ash) in a peat core, tentatively attributed to a source in the Ecuadorian Eastern Cordillera. Here, we present an investigation into the long-term controls on C accumulation in the oldest peatland reported in the Amazon basin. We develop a comprehensive, multiproxy palaeoecological dataset to (i) determine the developmental trajectory of the peatland and (ii) assess the peatland's response to past climate change.

2 | MATERIALS AND METHODS

2.1 | Study site

Aucayacu (3.927°S, 74.386°W), meaning “water of the natives” or “water of the warriors” in the language of the indigenous people, is a nutrient-poor ombrotrophic peat dome in Peruvian Amazonia (Lähteenoja & Page, 2011; Swindles et al., 2014). We estimate the

maximum dimensions of Aucayacu to be 33 km (NW-SE) \times 15 km (NE-SW). The vegetation of the site is characterized by pole and dwarf forest (including some palm trees) with an understory of grasses and ferns. The peatland developed between the Aucayacu stream of the Pastaza fan and the Tigre River (Figure 1). It is situated in the PMFB which formed during the uplift of the Andes Mountains and contains alluvial deposits several kilometres thick that began to accumulate in the Cretaceous period (Räsänen, Salo, Jungnert, & Pittman, 1990). The PMFB foreland basin is characterized by migrating river channels and avulsions leading to burial and erosion of peats (Lähteenoja et al., 2012). In Iquitos (120 km east of the study site), average rainfall of up to 3,000 mm/year is typical (Martinez et al., 2011). The average annual temperature at Iquitos is 26°C, with a diurnal range of approximately 10°C (30–32°C daytime temperature and 21–22°C at night) (Met Office, 2011).

2.2 | Fieldwork

Aucayacu was visited in 2008 (by O.L.) and a 3.5-km-long transect from edge to centre was established (Lähteenoja & Page, 2011; Lähteenoja et al., 2012). Peat thickness was determined using a Russian D-section corer with a 50-cm-long chamber (De Vleeschouwer, Chambers, & Swindles, 2010; Jowsey, 1966) across the transect (eight cores). The topography of the site was determined using a method involving two wooden stakes and a 35-m hose filled with water (for further technical details, see Lähteenoja, Ruokolainen, Schulman, & Alvarez, 2009; Lähteenoja, Ruokolainen, Schulman, & Oinonen, 2009). Accelerator mass spectrometry (AMS) radiocarbon dates were obtained from basal peat from the centre of the site (3.5 km from the edge, ca. 8.9 ka BP, Lähteenoja et al., 2012). Root remains were removed from the samples before acid-alkali-acid

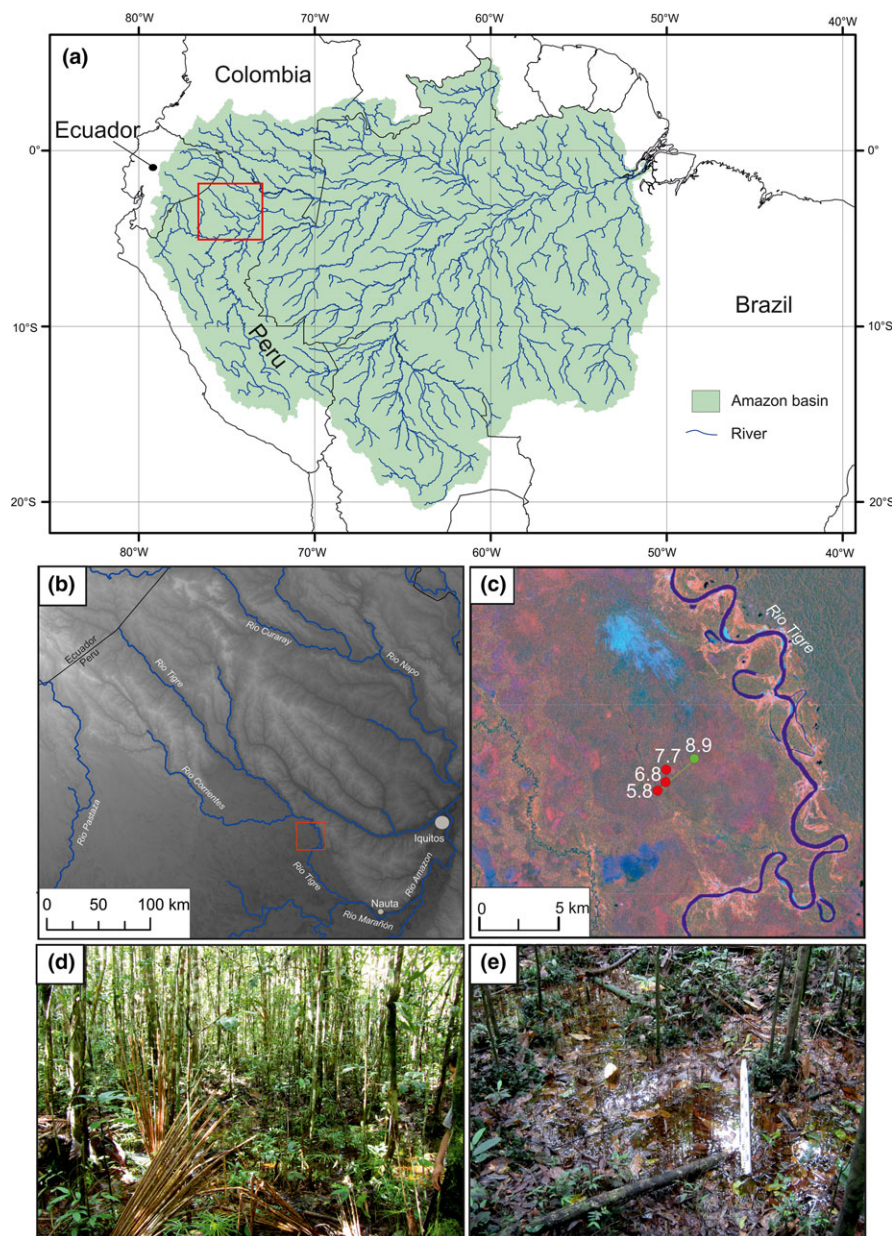


FIGURE 1 (a) Map of the Amazon Basin showing major rivers (with upstream catchment area >4 km²) derived from HydroSHEDS flow direction data at 30 min resolution (Lehner, Verdin, & Jarvis, 2006). The red box indicates the extent of panel (b). (b) SRTM digital elevation model of the region at 30 m resolution, showing the major rivers, population centres, and national borders. The red box indicates the extent of panel (c). (c) False colour Landsat 5 TM image (15 September 2011) of the Aucayacu peatland with bands 4, 5, and 3 assigned to R, G, and B, respectively. Wetter soil appears darker and the variation of vegetation type and condition is visible as variations in hues (brown, green, and orange) and tone. Both (b) and (c) available from the U.S. Geological Survey <http://earthexplorer.usgs.gov/>. (d) Photograph of the pole forest typical of Aucayacu peatland. (e) Pool microform in the centre of Aucayacu (a 1-m levelling staff is shown for scale)

pretreatment. Dating was carried out in the Laboratory of the Finnish Museum of Natural History, University of Helsinki, Finland.

For the purpose of this study, the site was revisited in 2011 (by G.T.S) and peat thickness was determined along an alternative 1.4-km-long transect (11 cores) using a 5-cm diameter Russian D-section corer in the same manner as in 2008 (De Vleeschouwer et al., 2010). Basic core stratigraphy was logged in the field using Troels-Smith (1955). A 5.3-m core was extracted from the interior of the Aucayacu peatland for a detailed multiproxy analysis. The core was taken from a flat area ("litter flat"—see Swindles et al., 2014) between pools. Two additional cores were logged in the central area (20 m apart) to examine the representativeness of the master core chosen for detailed analyses. Following clearance of vegetation along the narrow transect, the site was surveyed to the river edge using a Leica optical level and staff. Sampling locations were recorded by hand-held GPS. The size and shape of each microform along with the vegetation composition (within an area of 25 m²) as well as % litter and vegetation cover were recorded at each location.

A hole was augered at each sampling point and water level measured at regular intervals until it equalized to determine depth to water table. Water-table measurements were carried out over a 3-day period. pH and conductivity measurements were carried out on water samples extracted from the boreholes using calibrated field metres. Litter samples of approximately 5 cm³ were sampled from each point and placed into Ziploc bags. Samples were shipped to the University of Leeds and stored at 4°C prior to further analysis. Approximately one half of each surface litter sample was weighed, oven dried, burnt in a muffle furnace, and reweighed to determine moisture content and loss-on-ignition. The other half was used for analysis of contemporary testate amoebae (see Swindles et al., 2014).

2.3 | Chronology

Accelerator mass spectrometry ¹⁴C dates were carried out on basal peat samples and throughout the main core. Samples were sieved at 63 μm (retaining the <63 μm fraction) and all rootlets were picked out before acid-alkali-acid treatment. In some horizons hand-picked wood and peat macrofossils were dated (Table 1). ¹⁴C dating was carried out at the UK Natural Environment Research Council's Radiocarbon Facility (East Kilbride, UK), ¹⁴CHRONO (Queen's University Belfast), and Direct-AMS (Bothell, USA). All dates are reported as calibrated ages (cal. years BP, before present = AD 1950). Calibration was carried out using Calib 7.1 and the IntCal13 calibration dataset (Reimer et al., 2013). ²¹⁰Pb measurements were performed on contiguous 2 cm samples from the upper 50 cm of the Aucayacu core. ²¹⁰Pb methods followed modified versions of Ali, Ghaleb, Garneau, Asnong, and Loisel (2008) and Pratte, Mucci, and Garneau (2013). ²¹⁰Pb was extracted from 0.5 g of ground, freeze-dried peat, spiked with a ²⁰⁹Pb tracer, using sequential HNO₃-H₂O₂-HCl digestions with interspersed drying. The samples were then recovered in a 0.5 M HCl solution and plated to Sterling Silver discs over a 24-hr period. Samples were counted using an

Ortec Octète Plus Integrated Alpha-Spectrometry System with Maestro software at the Geography Radiometry Laboratory, University of Exeter. A constant rate of supply (CRS) model was used to assign ages to the raw ²¹⁰Pb activity profile (Appleby, 2001). Microscopic tephra layers have been reported from Aucayacu (Watson et al., 2015); however, these were not used in the chronology owing to the current uncertainty of their exact origin and age. Age models based on the ¹⁴C and ²¹⁰Pb ages were constructed using *Bacon*, a Bayesian piece-wise linear accumulation model, where the accumulation rate of sections depend to a degree on that of the preceding sections (Blaauw & Christen, 2011). The a priori accumulation rate was assumed to be 15 year/cm and 5-cm thick sections were used. Markov chain Monte Carlo (MCMC) iterations estimate the accumulation rate for each of these sections.

2.4 | Sedimentology

Grain size frequency distribution for 93 different grain size classes, ranging from 0.4 to 2000 μm, were determined for sediment samples below the peat using a Beckman Coulter LS 13 320 Laser Diffraction-Particle Size Analyser equipped with a Universal Liquid Module. Utilizing a protocol modified from van Hengstum, Reinhardt, Boyce, and Clark (2007) and Murray (2002), 30% H₂O₂ was added to subsamples in a 80°C water bath to oxidize organic matter (OM). HCl treatment was deemed unnecessary owing to low carbonate content. End-member mixing analysis (EMMA) was performed on the grain size analysis results to detect grain size variability in sediments beneath the peat at Aucayacu. EMMA was performed following the procedure of Dietze et al. (2012, 2014) using extensions implemented in the R package EMMAgeo (Dietze & Dietze, 2013). Only robust end members (EMs) were included, defined as those with nonoverlapping, interpretable EM loadings, with the addition of those in which similar EM loadings occurred in most of the model runs (Dietze et al., 2014). EM scores were centred and scaled using the "deconstand" function in the R package "vegan" (Oksanen et al., 2013). A Euclidean distance matrix was generated using the "dist" function in the R package "stats" (R Core Team, 2016). The loadings were scaled to be genetically meaningful (scale and unit according to original data: Weltje, 1997) using a weight transformation after Klován and Imbrie (1971).

2.5 | Pollen analysis

Samples measuring 1 cm³ were processed using standard protocols (Fægri & Iversen, 1989), including sieving at 250 μm to remove large organic fragments and a cold HF treatment to dissolve silicates. Pollen were not sieved at 10 μm because of the presence of *Cecropia* and other pollen types with small grains (<10 μm). Residues were dehydrated with isopropanol and mounted in silicone oil. Three hundred pollen grains were identified and enumerated in each sample. Spores and pollen from obligate aquatic plants are not included in the pollen sum. Abundance of all pollen and spores was calculated relative to the pollen sum. Over 185 pollen taxa were differentiated,

TABLE 1 ^{14}C dates from Aucayacu including as transect of basal ages and the main multiproxy core

Laboratory code	Depth (cm)	Distance from river (m)	^{14}C age	1 σ error	Material dated	$\delta^{13}\text{C}$ (per mil)	Calibrated range 2 σ (cal. year BP)	Calibrated median age (cal. year BP)
Master core								
SUERC-46946	21	1,400	70	37	Wood fragments	-28.9	266–22	124
SUERC-46947	30	1,400	133	37	Wood fragments	-27.6	269–6	136
SUERC-46952	41	1,400	146	37	Wood fragments	-30.7	277–0	149
UBA-20284	50	1,400	786	22	Wood and leaf macrofossils	-31.7	726–677	705
D-AMS-011347	64	1,400	2,372	23	Sieved peat, roots removed	-33.5	2,424–2,345	2,381
D-AMS-011348	77	1,400	2,783	32	Sieved peat, roots removed	-30.1	2,943–2,793	2,882
SUERC-59689	90	1,400	3,549	37	Sieved peat, roots removed	-29.4	3,896–3,717	3,843
SUERC-46949	101	1,400	3,732	37	Wood fragments	-27.2	4,149–3,977	4,084
SUERC-59690	160	1,400	4,222	36	Sieved peat, roots removed	-29.9	4,847–4,629	4,749
D-AMS 011350	179	1,400	5,191	35	Sieved peat, roots removed	-32.1	5,988–5,898	5,948
SUERC-59691	200	1,400	5,625	37	Sieved peat, roots removed	-29.8	6,447–6,314	6,405
D-AMS 011352	249	1,400	5,565	27	Sieved peat, roots removed	-33.9	6,396–6,303	6,353
SUERC-59692	276	1,400	5,988	37	Sieved peat, roots removed	-29.2	6,884–6,738	6,828
SUERC-59693	300	1,400	6,825	39	Sieved peat, roots removed	-29.9	7,682–7,588	7,657
Basal date transect								
D-AMS-011353	120	77	5,016	28	Sieved peat, roots removed	-27.8	5,891–5,658	5,751
D-AMS-011354	300	749	6,004	34	Sieved peat, roots removed	-31.5	6,938–6,749	6,844
SUERC-59693	300	1,400	6,825	39	Sieved peat, roots removed	-29.9	7,725–7,587	7,656
*Hela-2216/1	750	3,500	7,949	50	Sieved peat, roots removed	-29.4	8,990–8,640	8,815
*Hela-2216/2	750	3,500	7,976	50	Sieved peat, roots removed	-29.4	8,999–8,649	8,846

Dates marked with an asterisk were published previously in Lahteenoja et al. (2012).

but we present the 13 most important types as determined through principal components analysis. The full palynological dataset will be presented elsewhere.

2.6 | Plant macrofossils

Plant macrofossils were analysed at 5 cm intervals. Samples were washed and sieved under a warm-water spray using a 0.20-mm mesh sieve. The volume percentages of different vegetative remains (rootlets, leaves, wood fragments) were estimated to the nearest 5% with a stereoscopic microscope. Macroscopic charcoal pieces (>1 mm) were counted during plant macrofossils analysis. The number of seeds and insect remains were counted separately and expressed as absolute numbers. The volume percentage of amorphous or unidentifiable organic matter (UOM) was estimated to the nearest 5% during sieving and serves as a complimentary indicator of peat decomposition (Gałka et al., 2013).

2.7 | Phytoliths and diatoms

Ashes remaining after loss-on-ignition (see below) were mounted on glass slides and phytolith and diatom total abundance were determined (number of diatoms in 1 cm³ sample of peat). Phytoliths were classified based on their general morphology.

2.8 | Testate amoebae and hydrological reconstruction

Full details of the testate amoeba method and analysis are provided in Swindles et al. (2014), Swindles, Lamentowicz et al. (2016), and Swindles, Morris et al. (2016). Subfossil testate amoebae were counted under transmitted light at 200–400 \times magnification and identified using morphology, composition, size, and colour to distinguish taxa. The weighted-averaging partial least squares (component 3) transfer function of Swindles et al. (2014) was applied to the subfossil testate amoebae to generate a water-table reconstruction. This model has the following performance statistics: $r^2_{\text{(apparent)}} = 0.81$; RMSE = 3.81 cm; $r^2_{\text{(leave-one-out-crossvalidation)}} = 0.65$; RMSEP = 5.24 cm; water-table depth range = 49 to -12 cm (negative values indicate a water level above the ground surface). Because the transfer function is based on one-time water-table measurements, the reconstruction was detrended using linear regression following Swindles et al. (2015).

2.9 | Peat properties and C accumulation

The main core was subsampled in contiguous 1-cm sections, and moisture content and loss on ignition (LOI; ash content) were determined using standard methods on 1 cm³ samples of peat (Chambers,

Beilman, & Yu, 2011). Bulk density was calculated by dividing sample mass after freeze-drying by volume (Chambers et al., 2011). The change in sample mass after drying also provided a measurement of moisture content. C and N were measured on a Thermo Scientific Flash 2000 Series CHNS/O Analyser. Peat accumulation rate (mm/year), C accumulation rate ($\text{g C m}^{-2} \text{ year}^{-1}$), and the long-term average rate of C accumulation (LORCA) were calculated following Tolonen and Turunen (1996). Peat humification analysis was carried out through colorimetric measurement of alkaline extracts following Roos-Barraclough, van der Knaap, van Leeuwen, and Shotykh (2004). This proxy has come under criticism (e.g., Yeloff & Mauquoy, 2006), so we adopt it cautiously here.

2.10 | Rock-Eval pyrolysis

We used Rock-Eval[®] 6 pyrolysis to analyse organic constituents of the peats and underlying sediments (Vinci Technologies, Rueil-Malmaison, France; Lafargue, Espitalité, Marquis, & Pillot, 1998). The Rock-Eval[®] 6 instrument pyrolyses OM under an inert (N_2) atmosphere and oxidizes OM at programmed temperature heating of bulk sediments (~20 mg) at a heating rate of 25°C/min. Rock-Eval[®] 6 pyrolysis measures total organic C (TOC, wt.%) as well as the quantity of labile, readily degradable hydrocarbon devolatilized at 300°C (S1, mg hydrocarbon/g), higher molecular weight kerogen-derived hydrocarbon released by thermal cracking of OM at 650°C (S2, mg hydrocarbon/g), and the amount of carbon dioxide released during pyrolysis of kerogen (S3, mg hydrocarbon/g). Following pyrolysis, the sample is automatically transferred to an oxidation oven where it is heated from 400 to 850°C, incinerating all of the residual carbon in the sample (RC wt.%). The quantity of all OM released during pyrolysis and oxidation heating is the total organic carbon (TOC; wt.%). Analyses of standard reference materials (IFP 160000, Institut Français du Pétrole and internal 9107 shale standard, Geological Survey of Canada, Calgary) show accuracy and precision to be better than 5% relative standard deviation. In near-modern sediments, the S1 fraction of OM mainly consists of readily degradable geolipids and pigments predominantly derived from autochthonous OM (e.g., algal-derived lipids; Carrie, Sanei, & Stern, 2012). Lipid material consists of the fraction of OM isolated from biological material by extraction with organic solvents (Meyers & Ishiwatari, 1993). Biological lipids undergo degradative alteration as the algae sinks to the bottom of water bodies. After sedimentation, molecular composition is modified diagenetically to various degrees depending on the composition of the parent lipid, resulting in slightly different compounds termed “geolipids” (Meyers & Ishiwatari, 1993). S2 compounds in near-surface sediment are derived from the highly aliphatic biomacromolecule structure of algal cell walls and aquatic biological matter (Carrie et al., 2012; Sanei, Stasiuk, & Goodarzi, 2005). The S3 portion of OM is dominated by carbohydrates, lignins, and other remains of terrigenous plant materials (Carrie et al., 2012). Humic and fulvic acids are also represented in the S3 fraction (Albrecht, Sebag, & Verrecchia, 2015). Residual carbon represents refractory carbon (RC: charcoal, coal, reworked, oxidized OM) that cannot be further modified by

bacterial activity in early diagenesis. Oxygen index (OI—the amount of oxygen relative to the amount of organic carbon present in a sample) and hydrogen index (HI—the amount of hydrogen relative to the amount of organic carbon present in a sample) were calculated as follows: $\text{OI} = \text{S3}/\text{TOC} \times 100$; $\text{HI} = \text{S2}/\text{TOC} \times 100$.

2.11 | Statistical analysis

Fossil pollen data were zoned using stratigraphically (depth)-constrained cluster analysis by incremental sum of squares (CONISS). Three statistically significant zones were identified using the broken stick model (Bennett, 1996). These zones were marked onto the proxy diagrams and used to interpret the main phases of peat development. CONISS was carried out on the full pollen dataset and also the 13 most important types—identical results were obtained. CONISS was also used to determine contemporary vegetation zones using distance along transect as the constraining variable. Nonmetric multidimensional scaling (NMDS) analysis using the Bray–Curtis distance was applied to contemporary vegetation data to help determine the main communities. Statistically significant ($p < .05$) environmental variables were fitted using Envfit, which is a routine for fitting an environmental vector onto an ordination. CONISS was also undertaken on the EMMA results to determine variability in the EM scores. Statistical analyses were carried out using PAST (Hammer, Harper, & Ryan, 2001) and the RIOJA (v. 0.9) and VEGAN (v. 2.3) packages in R v. 3.2 (Juggins, 2015; Oksanen et al., 2013).

2.12 | Climate data and modelling

Full details of climate data and modelling procedures including hindcasts and future scenarios used here are provided in Appendix S1.

3 | RESULTS

3.1 | Site characteristics

Hydrology, plant communities, and geochemistry are highly variable along the contemporary transect (Figure 2). Microforms are present in the peatland including pools containing standing water, hollows, litter flats, and litter hummocks/ridges (see Swindles et al., 2014). Sometimes litter hummocks were anchored on tree roots and were termed “tree hummocks.” The microforms are characterized by different water-table depths (Fig. S1). pH and conductivity suggest that Aucayacu is currently a nutrient-poor system and topographic survey data show that the site is clearly domed (Figure 2).

The most abundant trees include *Alibertia* sp., *Iryanthera ulei*, *Oxandra euneura*, *Virola pavonis*, and *Zygia* sp. The most commonly occurring palm trees are *M. flexuosa* and *Oenocarpus mapora*. The understory is dominated by the fern *Trichomanes pinnatum* and grass *Pariana* sp. Six vegetation zones occur across the site (Fig. S2). Beginning at the river edge and working towards the peatland interior, the vegetation zones comprise: A1 dominated by *O. euneura*, *Parahancornia peruviana*, *Lacmellea oblongata*, and *Eschweilera* sp. 1;

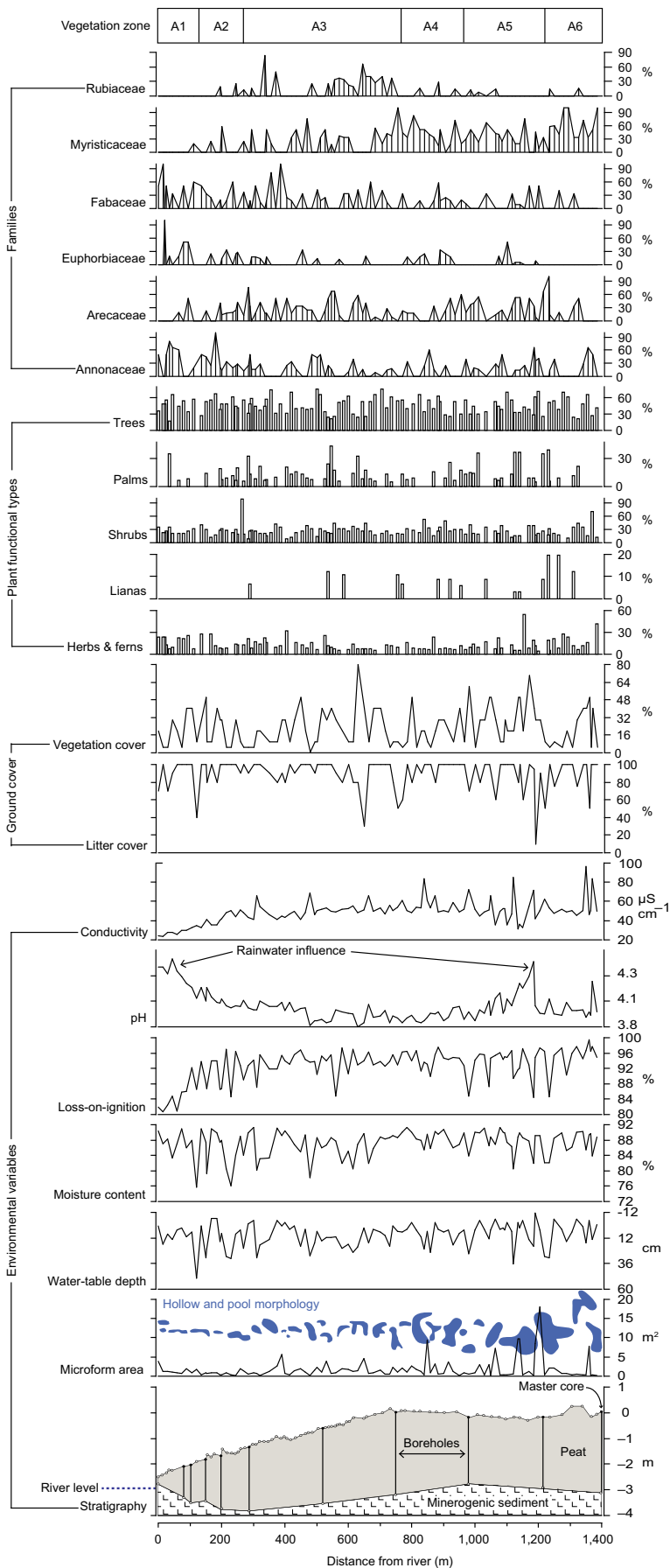


FIGURE 2 Topographic and stratigraphic profile of the Aucayacu peatland with environmental variables and ecological data (plant families and plant functional types) recorded along the transect. Data are plotted against distance from the Aucayacu stream. The shape (“hollow and pool morphology”) and calculated area of individual hollow and pool microforms are also shown (“microform area”). Vegetation zones are illustrated (see Fig. S2) [Colour figure can be viewed at wileyonlinelibrary.com]

A2 dominated by *Zygia* sp. 1, *O. euneura*, *M. flexuosa*, and *T. pinna-tum*; A3 dominated by *I. ulei*, *Zygia* sp. 1, *Alibertia* sp. 1, and *O. ma-pora*; A4 dominated by *I. ulei*, *Zygia* sp. 1, and *Alibertia* sp. 1; A5 dominated by *M. flexuosa*, *Zygia* sp. 1, *V. pavonis*, and *I. ulei*; and A6 dominated by *I. ulei*, *Brosimum* sp. 1 and *Euterpe precatoria*. The major environmental controls on vegetation distribution along the transect appear to be distance from the river and peat depth (Fig. S3).

3.2 | Peat initiation

We found progressively younger dates from the centre to the edge of the peatland: ca. 8.9 ka BP in the centre (7.5 m peat thickness; Lahteenoja et al., 2012), ca. 7.7 and 7.1 ka BP midway (~3.0 m peat thickness), and ca. 5.6 ka BP at the edge (1.2 m peat thickness).

3.3 | Core stratigraphy

Peat depth across the transect varies from <1 to >3 m (Figure 2). Further to the northeast, peat depths of ~7.5 m have been recorded (Lahteenoja et al., 2012). The stratigraphy of the three logged cores is similar and contains alternating bands of humified peat with occasional wood and wood-dominated peat (Fig. S4). There is a horizon of increased minerogenic material in the middle of the peat units in all three cores. Underlying the peat are sediments dominated by silt and clay, in turn overlying very coarse silt with fine sand.

3.4 | Sedimentology

Results from EMMA are provided in Figs S5–S9 and Tables S1–S3. EMMAgeo identified that the maximum number of EMs was 7. Values of the weight transformation that explained the most variance ranged from 0.00 to 0.26, with 0.00–0.06 performing the best. We chose a model using a weight transformation of 0 and consisting of four robust EMs. The EMMA model explained $78 \pm 18\%$ of the mean total variance across subsamples and $82 \pm 15\%$ of the mean total variance across the grain size distribution (GSD). Significant breaks occur between 497 and 498 cm and between 492 and 493 cm. The first break represents the disappearance of EM-070, while the second break represents the disappearance of EM-112. The core displays a fining-upward succession that is consistent with the interpretation of progressive isolation from the main channel flow over time as EM-012 and EM-05 can only be deposited in quiet water conditions. The basal section of the core represents a depositional environment dominated by very coarse silt and fine sand where finer sediments were not deposited. This is interpreted as a relatively higher energy environment than the subsequent setting where finer sediments were deposited.

3.5 | Core chronology and peat accumulation rates

Information from ^{14}C dates and ^{210}Pb determinations on the central Aucayacu core are provided in Table 1 and Fig. S10. The ^{14}C dates

were in stratigraphic order apart from one date at 200 cm: SUERC-59691 (Table 1). The Bayesian age–depth model is shown in Figure 3 and illustrates changes in peat accumulation rate through time. Peat accumulation rate varies between 0.05 and 18.2 mm/year (mean = 1.88 mm/year) (Figure 4). A phase of extremely slow peat accumulation, possibly a hiatus, is apparent between 50 and 60 cm, and phases of rapid accumulation occur at 244–265, 109–137 cm, and above 40 cm. The apparent rapid accumulation rate in the uppermost 40 cm reflects the larger proportion of fresh, undecomposed litter at the top of the peat profile, where peat has not yet undergone substantial decomposition (Figures 3 and S10).

3.6 | Pollen analysis

Changes in pollen and spore abundance over time reflect three phases of peat development: open water wetland (310–270 cm), forest swamp (270–95 cm), and raised peat dome (above 95 cm) (Figure 5). The open water wetland phase is dominated by arboreal pollen, with consistently high abundances of Moraceae/Urticaceae (23%–24%), particularly *Pseudolmedia*, *Brosimum*, and *Helicostylis* types, likely derived from floodplain forest communities surrounding slow-moving open water, most likely an oxbow lake or backwater pond that was permanently inundated. The abundance of Poaceae (4%–19%) and Cyperaceae (5%–16%) pollen reflects an open water wetland environment that supported semiaquatic species of these families, rather than terrestrial forms (Burn, Mayle, & Killeen, 2010). This is supported by the absence of other terrestrial herb pollen types.

The presence of evergreen tree pollen in this zone indicates a closed canopy forest around the water body. Similarly, trees from the genus *Cecropia* (12%–51%) require light gaps, can tolerate flooded conditions, and frequently occupy low- to midlevel communities in floodplain forests, especially várzea forest (Nebel et al., 2001; Worbes, 1997). Clay content in this phase (as observed in the pollen slides and loss-on-ignition data) is higher than in successive zones, suggesting a low-energy depositional environment probably not directly connected to the river at this time.

The forest swamp phase is characterized by an increase in *Mauritia/Mauritiella* pollen, likely reflecting the high water level of a floodplain environment. *Mauritia flexuosa* is adapted to flooded conditions and has pneumatophores and other anatomical adaptations to enable gas exchange in inundated ground surface conditions (Junk, 1989). The abundance of *Cecropia* pollen in this zone suggests that although the water level was relatively shallow, seasonal flooding was common because *Cecropia* seedlings will not establish under permanent inundation (Junk, 1989), and trees of this genus are most common in midlevel floodplain plant communities (Nebel et al., 2001; Worbes, 1997). Pollen of Combretaceae/Melastomataceae is most abundant in this phase (4%–30%). Although this pollen type encompasses a large number of species from two ubiquitous Neotropical families, a comparison of pollen signatures from a range of Amazonian forest formations shows that seasonally inundated rainforest is characterized by this pollen morphotype (Burn et al., 2010). The forest swamp

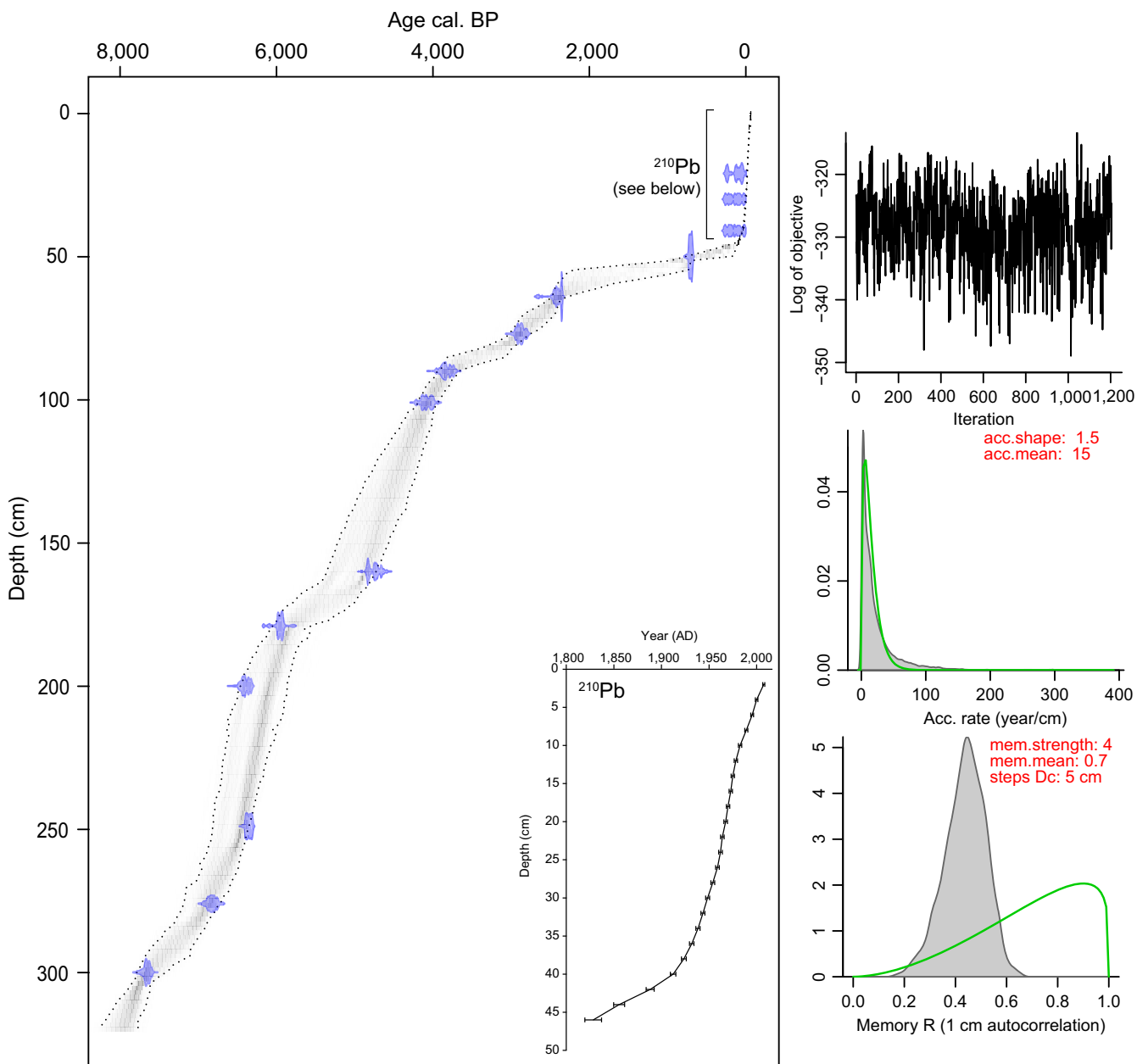


FIGURE 3 Bayesian age–depth model of the Aucayacu core. On the right-hand panel, the top plot shows that both MCMC runs were stable, the middle plot show the prior (curves) and posterior (filled histograms) distributions for the accumulation rate (year/cm), and the bottom plot show the prior (curves) and posterior (filled histograms) for the dependence of accumulation rate between sections. The large plot shows age distributions of calibrated ^{14}C dates and ^{210}Pb , and the age–depth model (grey scale). Dark grey areas indicate precisely dated sections of the chronology, while lighter grey areas indicate less chronologically secure sections. The ^{210}Pb age model is also shown (insert) [Colour figure can be viewed at wileyonlinelibrary.com]

phase characterized by this pollen type therefore likely reflects a seasonally inundated floodplain forest. The depositional environment likely contained no permanent water body, as indicated by the decline in Poaceae and Cyperaceae pollen at the boundary between this zone and the previous zone.

Mauritia/Mauritiella (10%–42%) and more than 10 additional undifferentiated *Arecaceae* pollen types dominate the assemblages above 95 cm, indicating the transition to the final peat dome phase. The transition from seasonally inundated floodplain forest to a

nutrient-poor peatland is indicated, as *Combretaceae/Melastomataceae* and *Cecropia* pollen (reflective of seasonally inundated floodplain forest) decline in this zone. Other abundant taxa include *Alchornea/Aparisthium* (*Euphorbiaceae*) (2%–15%) and *Virola* (*Myricaceae*) (4%–22%), species of which produce hypertrophic lenticels and adventitious rooting systems (Junk, 1989; Lopez & Kursar, 2003) in response to low-oxygen conditions caused either by inundation and/or burial by sediments or peat. *Virola* pollen is indicative of peatland in the Neotropics (Ledru, 2001). Pollen and LOI data

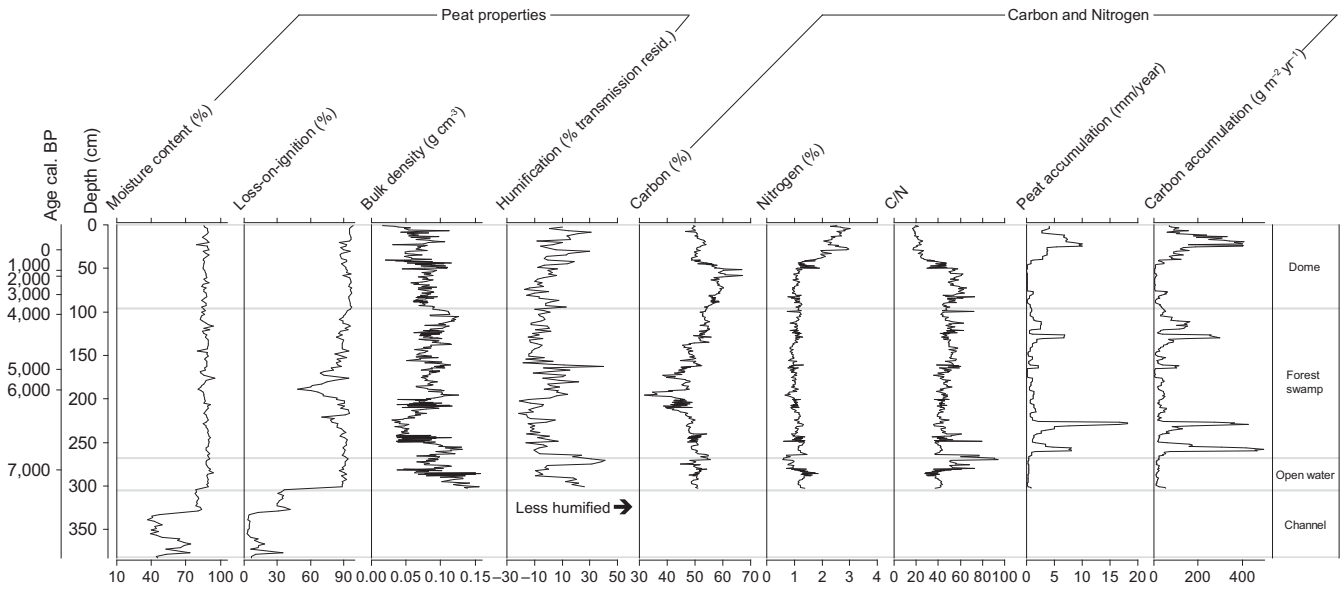


FIGURE 4 Peat properties and carbon and nitrogen data from the Aucayacu core, plotted by depth and age. Interpretative zones are shown on the right-hand side of the diagram

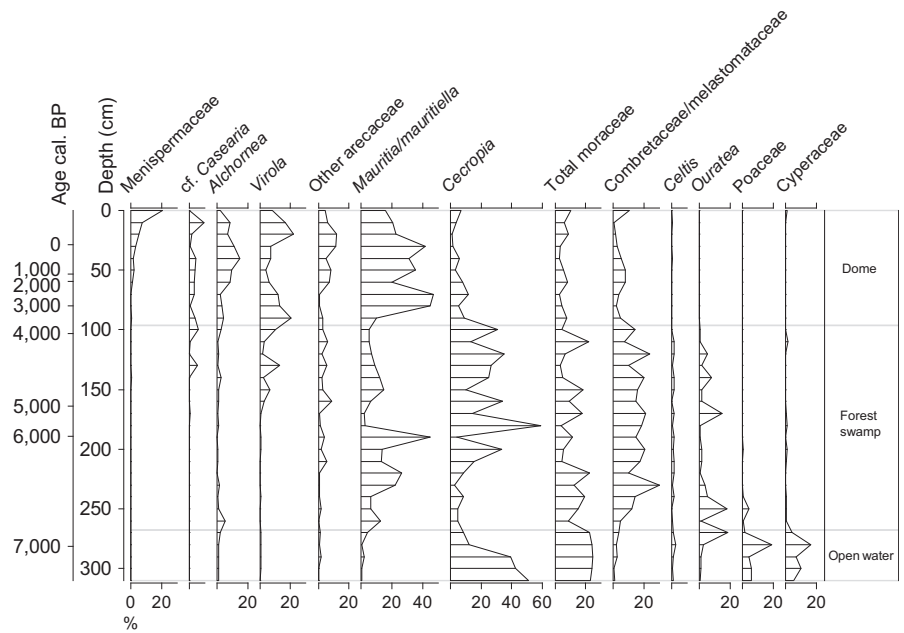


FIGURE 5 Percentage pollen data from the Aucayacu core, plotted by depth and age. Interpretative zones are shown on the right-hand side of the diagram

(Figures 4 and 5) suggest that in this phase the peatland mostly functioned as an ombrotrophic dome; however, the occasional influence of high-magnitude floods cannot be discounted.

3.7 | Peat composition and macrofossils

An analysis of macrofossils shows considerable variation in the proportional contributions of roots, wood, UOM, and leaf epidermis (Figure 6). Major shifts in root-dominated to wood-dominated peats are apparent during the forest swamp phase. Occasional seeds and insect remains are also present, and quartz grains were found in the

bottom of the profile. Macroscopic charcoal occurs in the uppermost 20 cm of the core, and at 73 and at 123 cm. Phytoliths are also common. In particular, an increase in spinulose palm phytoliths (produced by members of the Arecaceae family) occurs in the peat dome phase. Diatoms are present in three depths in the core and may suggest wetter conditions at these times (Figure 6).

3.8 | Testate amoebae

The most common testate amoebae in the profile include *Hyalosphenia subflava*, *Trigonopyxis arcula*, *Phryganella acropodia* and

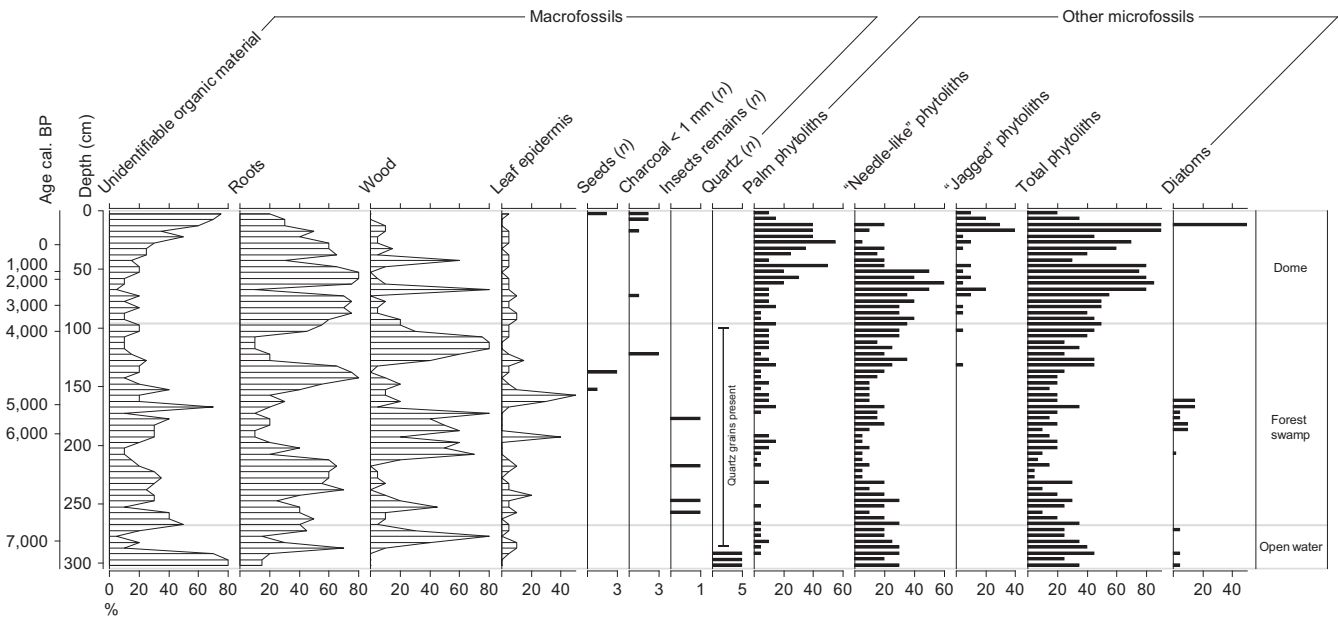


FIGURE 6 Peat composition data (plant macrofossils) and other microfossils found in the Aucayacu core, plotted by depth and age. Interpretive zones are shown on the right-hand side of the diagram

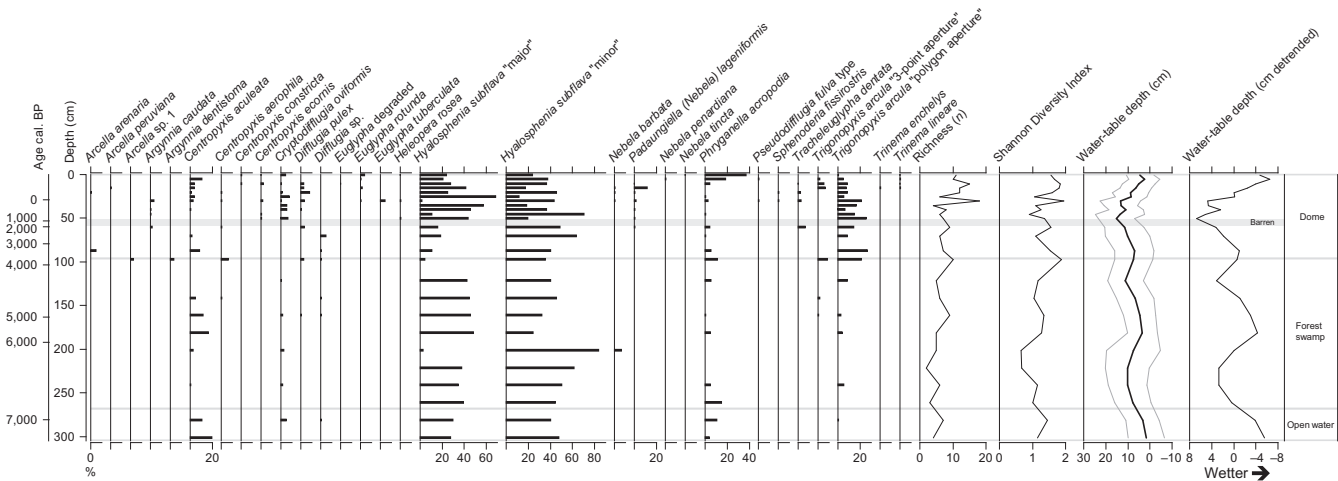


FIGURE 7 Subfossil testate amoebae diagram from Aucayacu (data are expressed as percentages). Richness, Shannon diversity index values and the water-table reconstruction (plotted with errors derived from bootstrapping and as detrended values) are also shown

Centropyxis aculeata. Preservation down-core is variable and concentrations of testate amoebae in general were very low (see Swindles, Lamentowicz et al., 2016; Swindles, Morris et al., 2016). The horizon 50–60 cm (peat dome phase) was barren of testate amoebae.

A contemporary training set from Aucayacu (Swindles et al., 2014) shows that *C. aculeata* is an indicator of surface water; an abundance of this taxon in the early part of our record indicates persistent standing water and provides evidence to support the open water depositional environment interpreted from pollen analysis. Fluctuations in palaeohydrological conditions during the subsequent forest swamp phase and a trend towards dryness followed by a wet shift (at ca. 50 cm) in the peat dome phase are identified from the testate amoeba-based reconstruction (Figure 7).

3.9 | Peat properties and C accumulation

Loss-on-ignition (LOI) data clearly show first peatland initiation at ~300 cm (Figure 4). Relatively lower LOI values during the forest swamp phase provide clear evidence for episodes of minerogenic input. Within the peat (0–300 cm), the maximum LOI is 98.4% and the minimum is 48.3% (mean = 88.6%). Above 96 cm (the peat dome phase), the maximum LOI is 98.4% and the minimum is 88.5% (mean = 93.9%). However, ash content above 96 cm is related to the high abundance of silica phytoliths rather than minerogenic material (see Figure 6). The bulk density of the peat varies between 0.02 and 0.16 g/cm³ (mean = 0.08 g/cm³). Several shifts in peat humification are apparent with major excursions to lower

humification at 264–280 cm, 156–199 cm, and above 40 cm (Figure 4). These may relate to either wetter episodes where peat humification was reduced or changes in peat composition (e.g., shift from root and wood-dominated to UOM-dominated peat—Figure 6). The C/N (% mass) varies between 16.2 and 94.1 (mean = 44.9). The large increase in %N in the uppermost 40 cm of the profile reflects the oxic zone, where peat has not yet fully decomposed. A decrease in %C in the forest swamp phase reflects the incorporation of minerogenic material within the peat.

C accumulation rates mirror peat accumulation rates, with a phase of extremely slow accumulation at 50–60 cm, and phases of rapid accumulation at 244–265 cm, 109–137 cm, and above 40 cm. C accumulation rates vary between 1.8 and 495.7 g C m⁻² year⁻¹ (mean = 70.8 g C m⁻² year⁻¹). LORCA is 15.96 g C m⁻² year⁻¹, which is lower than the 39 g C m⁻² year⁻¹ found by Lähteenoja et al. (2012) on the longer core (7.5 m) taken 2.1 km to the north-east.

3.10 | Rock-Eval pyrolysis

S1 C displays a decreasing trend down-core, which most probably relates to diagenesis of labile OM as S1 C is the most readily degradable fraction of organic C (Figure 8). Both S1 and S2 C increase during the early open water wetland phase. This is likely attributable to the relative increase in wetter conditions that promoted primary production and enhanced preservation of OM. Increases in S3 C during the lower part of the open water wetland phase likely represent increased delivery of terrestrially derived OM from increased runoff or more frequent floods. The shifts in S1, S2, S3, and C/N ratio during the open water wetland phase (Figures 4 and 8) suggest a transition to more lacustrine conditions, reflecting

the isolation of the water body through time. S1/S2 illustrates selective diagenesis of S1 relative to S2. RC/TOC shows relative decline in proportion of refractory C during the open water wetland phase and in the uppermost peat. This is attributed to a relative increase in proportion of more labile, liptinitic-rich, and autochthonous OM (S1 and S2). RC/TOC remains relatively constant throughout the forest swamp phase, with around 70% of the TOC being refractory due to humification occurring in the uppermost layers of the peatland.

Fluctuations in HI and OI profiles during the open water wetland phase reflect the shift in depositional environment from one that accumulated under more terrestrial conditions (Type III OM, OI of ~140, and HI of ~200) to one that accumulated more autochthonous, liptinitic-rich C (Type II OM, HI 300–400 and OI of less than 50). In the uppermost 50–100 cm of peat, HI is elevated relative to deeper peats, although OI remains more or less constant. This suggests that the relative increase of HI is due to higher deposition of liptinitic-rich OM and little change in the proportion of terrestrially derived OM input. This shallow section may also reflect active humification that targets liptinitic-rich OM. The ratio RC/TOC shows downward enrichment of refractory OM as the more labile, hydrogen-rich, liptinitic fraction is degraded due to humification. In the uppermost 40 cm, the marked rise in OI is likely associated with the oxic zone and accumulation of humic and fulvic acids along with a labile geolipid fraction (S1).

4 | DISCUSSION

Our contemporary vegetation analysis suggests that water-table depth is not a strong control on modern vegetation distribution, illustrating that vegetation across the site is zoned at the meso-

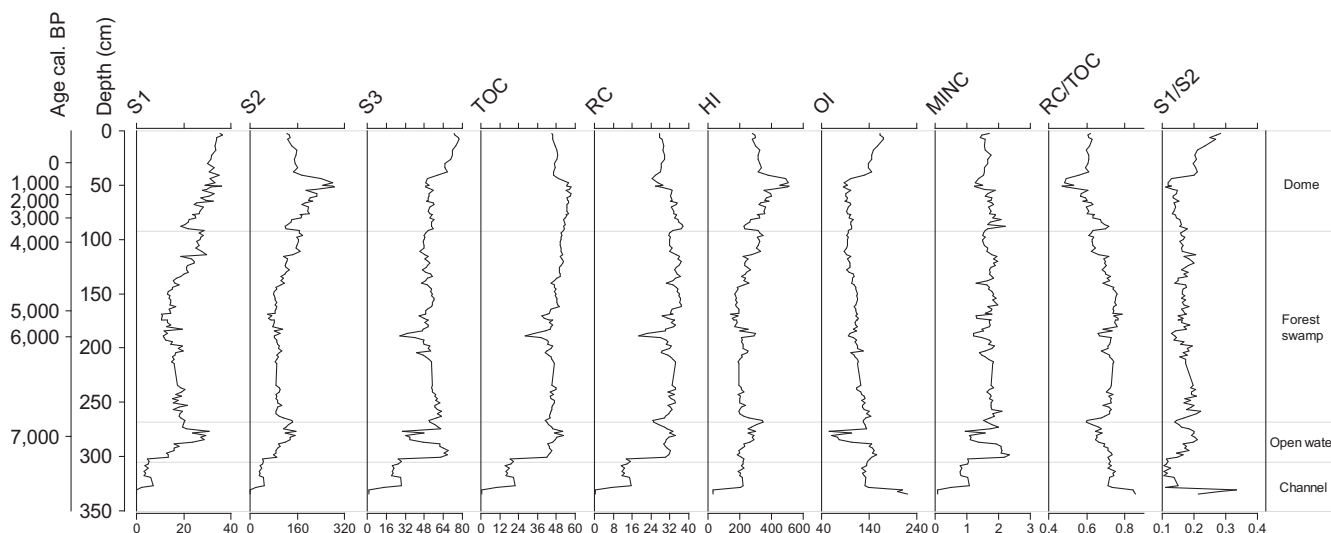


FIGURE 8 Rock-Eval pyrolysis data plotted by depth and age. Interpretative zones are shown on the right-hand side of the diagram. S1 = the free hydrocarbons present in the sample before thermal pyrolysis (in milligrams of hydrocarbon per gram of sample); S2 = the volume of hydrocarbons that formed during thermal pyrolysis of the sample; S3 = the amount of CO₂ (in milligrams CO₂ per gram of sample) produced during pyrolysis of kerogen (in milligrams CO₂ per gram of sample); TOC, total organic carbon (%); RC, residual carbon (%); HI, hydrogen index; OI, oxygen index; MINC, mineral carbon (%)

macroscale with distance from the river, unlike many northern peatlands that are commonly characterized by vegetation patterning at the microform level (e.g., Baird, Milner, Blundell, Swindles, & Morris, 2016). Our multiproxy palaeoenvironmental dataset illustrates the long-term dynamics of the oldest known peatland in the Amazon basin. The modern peat dome has developed in several distinct phases, and its dynamics were driven by a combination of autogenic (vegetation succession, vertical and lateral expansion) and allogenic (climatic, floodplain) influences on millennial and multicentennial time scales.

4.1 | Allogenic and autogenic controls on peatland development

Our multiproxy dataset suggests a relatively simple and unidirectional succession from open water wetland (ca. 7.8–6.6 ka BP), through inundated forest swamp (ca. 6.6–3.9 ka BP), to raised peat dome (since ca. 3.9 ka BP) (Figure 9). This is in contrast to the palynological study of Kelly et al. (2017) on another Amazonian ombrotrophic peatland (San Jorge), which suggested a much more complex trajectory with reversals to former states. The fining-upwards succession in the mineral sediments underlying the peat is consistent with the isolation of a river channel segment into an oxbow lake or a backwater following eastward migration of the river channel, which subsequently allowed peatland development.

Our four basal dates suggest that the peatland underwent a rapid lateral expansion (~2.0 m/year) from a central nucleus, before slowing down after ca. 7.7 ka BP (~0.7 m/year), and again after ca. 7.1 ka BP (~0.4 m/year) (Fig. S11). Alternatively, the peatland may have emerged in a more complex manner from several initiation centres that coalesced over time. Both of these point initiation and simultaneous initiation development pathways have previously been suggested for Northern peatlands (Belyea & Baird, 2006; Foster & Wright, 1990; Glaser, Hansen, Siegel, Reeve, & Morin, 2004). However, our four basal dates become monotonically younger from centre to margin, which is consistent with a point initiation and subsequent lateral expansion (Figures 1 and S11). As vegetation developed, peat accumulated and the system transitioned into an inundated forest swamp. After sufficient vertical accumulation of peat, the peat surface became hydrologically disconnected from the influence of river flooding, and the ecosystem transitioned into an ombrotrophic peat dome with less pronounced cycles between dry and flooded conditions. The timing of the first appearance of the contemporary pole forest is ambiguous in the pollen record because many of the characteristic trees of this vegetation type are insect-pollinated and are thus commonly poorly represented in palaeoecological records (e.g., Kelly et al., 2017). Furthermore, the pollen rain in pole forests is often overwhelmed by the presence of a relatively small number of *M. flexuosa* trees (e.g., Kelly et al., 2017). However, the presence of *Mauritia* pollen may also suggest the persistence of palm swamp vegetation disconnected from the influence of pronounced river flooding. The presence of charcoal in the core shows that these ecosystems have been affected by fire on at least three

occasions in the last 4,500 years, most probably related to anthropogenic activity (see McMichael, Correa-Metrio, & Bush, 2012). This is in contrast to other published records from peatlands in Peruvian Amazonia in which no charcoal has been found (see Kelly et al., 2017; Roucoux et al., 2013).

Although there are many uncertainties over the Holocene climate history of western Amazonia (see Flantua et al., 2016; Kelly et al., 2017), some climatic events for which independent evidence exists may have been recorded in the peat record at Aucayacu. During the forest swamp phase we identify two distinct dry phases at ca. 6.6–6.1 (henceforth drought phase A) and ca. 4.9–3.9 ka BP (drought phase B), as evidenced by a lack of aquatic testate amoebae and increased peat humification. In addition, an apparent hiatus in peat accumulation occurred between ca. 1.8 and 1.1 ka BP. Hiatuses in peat accumulation may occur in response to tree fall and tip-up events (Dommain et al., 2015), although high phytolith concentrations and a complete absence of preserved testate amoebae around the hiatus at Aucayacu suggest that it is more likely to reflect increased peat decomposition. This hiatus overlaps with the beginning of a similar hiatus identified at the San Jorge peatland 150–200 km away (ca. 1.3–0.4 ka BP; Kelly et al., 2017). Timings of drought phases A and B and the hiatus at Aucayacu are temporally consistent with known drought phases in Peru (Figure 9). For example, major drought phases have been identified in Lake Sauce in Peruvian Amazonia at ca. 4.9–3.5 ka BP and ca. 1.9–1.3 ka BP (Correa-Metrio, Cabrera, & Bush, 2010). Although the nature of strength of any teleconnection across the Andes is unclear, it is interesting to note that a major lowstand of Lake Titicaca also occurred between ca. 7 and 4 ka BP (Baker, Fritz, Garland, & Ekdahl, 2005).

Drought is thought to have been widespread across both upland and lowland Amazonia during the early–mid Holocene (Mayle & Power, 2008). A dry event is also recognized in other lakes of Peruvian Amazonia around the city of Puerto Maldonado between ca. 7.2 and 3.3 ka BP (Bush, Silman, & Listopad, 2007). Phases of reduced South American Summer Monsoon (SASM) rainfall have been dated at ca. 7–5 ka BP and ca. 1.5–0.9 ka BP (Bird, Abbott, Rodbell, & Vuille, 2011). Therefore, we interpret the hiatus as potentially reflecting a third drought phase (drought phase C). It is also interesting to note that drought phase B (ca. 4.9–3.9 ka BP) is contemporaneous with the well-documented and possibly global ca. 4.2 ka BP climate event (Booth et al., 2005; Davis & Thompson, 2006; Roland, Caseldine, Charman, Turney, & Amesbury, 2014), which itself is correlative with Bond Event 3 (Bond et al., 1997; Bond et al., 2001), although the mechanisms for global climatic teleconnection remain poorly understood.

The palaeoecological study of Peruvian Amazonian lake sediments by Bush et al. (2007) suggests that dry conditions during the mid-Holocene were followed by a period of increasingly wet conditions beginning between ca. 4.2 and 2.5 ka BP. A similar wet signal can be seen in our palaeohydrological reconstruction from Aucayacu, immediately following drought phase B. Drought phase C is also chronologically consistent with dry phases found in several other proxy records from Amazonia and other sites in South America

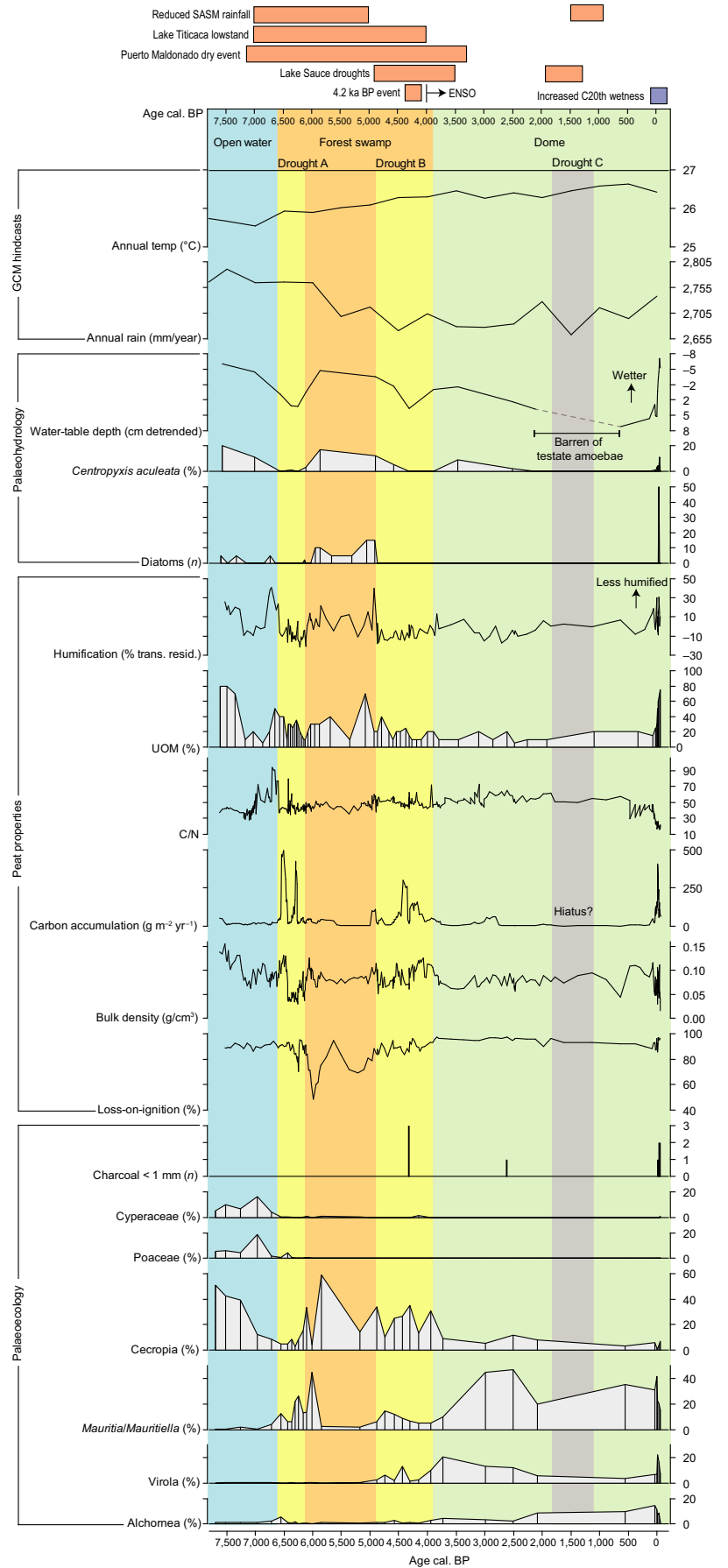


FIGURE 9 Summary diagram from Aucayacu illustrating the main phases of peatland development. Key climate events and GCM hindcasts (see text) are also illustrated

(Piperno & Becker, 1996; Roucoux et al., 2013; Weng, Bush, & Athens, 2002).

We observe differential effects of these droughts on peat and C accumulation regimes (Figures 9 and 10). During the forest swamp phase, drought phases A and B led to increased peat and C accumulation, whereas during the subsequent peat dome phase, drought phase C caused a collapse in peat and C accumulation. This apparent hiatus may be explained by recent research into the C dynamics of tropical peatlands. Hirano et al. (2012) investigated the C balance of drained and near-natural ombrotrophic tropical peatlands using eddy correlation. For a near-natural site, they found that gross primary production (P_G) showed a quadratic relationship with water-table depth. P_G was lowest at deep water-table levels (ca. 0.9 m below the ground surface), highest at intermediate water-table depths of ca. 0.3 m, and lower again (but not as low as for the deepest water tables) as water tables became shallower and the peatland surface became inundated. Ecosystem respiration (R_E —the sum of plant respiration and peat decay) also varied with water-table depth, being highest for deep water tables (0.9 m) and declining monotonically to inundation depths of up to 0.2 m, with the rate of decline increasing in the latter part of the water-table range.

Many other studies have shown how depth-integrated decay of peat (usually the dominant component of R_E) increases as the water table deepens (see Baird et al., 2017). The combined P_G and R_E data from Hirano et al. (2012) show that net rates of peat accumulation are highest when a tropical peatland is at its wettest and lowest when it is at its driest. Specifically, the data from Hirano et al. (2012) suggest that net accumulation of peat only occurs when water tables are shallower than ca. 0.3–0.2 m, while deeper water tables lead to a net loss of peat.

The increase in rates of peat accumulation during drought phases A and B (forest swamp phase) is the opposite of what occurs during drought phase C (peat dome phase). One possibility is that a reduction in water levels causes a sharp up step in productivity of the swamp vegetation—growth rates of the component species of this vegetation may normally be inhibited by the deep water-logged conditions that usually prevail—without a corresponding or matching

increase in rates of peat decay, which may be expected if water levels are still mostly near the peatland surface. Other possibilities can be conjectured, but what is needed is research on current swamp systems to see how they respond in terms of P_G and R_E during multiyear droughts. Different “rules” almost certainly apply to swamp and peat dome conditions given their different plant communities and the likely differences in the nutrient status of peat pore water, both of which will affect P_G and R_E (e.g., Debusk & Reddy, 2005; Rydin & Jeglum, 2006). It has also been shown that droughts can affect productivity in Amazonian forest communities in different ways (e.g., changes in biomass, autotrophic respiration, photosynthesis and tree mortality), and that they do not always cause a decrease in productivity (Doughty et al., 2015; Feldpausch et al., 2016). Such variations may offer an alternative explanation for our observations during the different drought phases.

A further observation is that drought phase A coincides with an ecosystem state shift from open water wetland to forest swamp (ca. 6.6 ka BP); and drought phase B with a shift from forest swamp to raised peat dome (ca. 3.9 ka BP) (Figures 9 and 10). GCM hindcasts of annual average precipitation also suggest a slight drying trend between the open water wetland and forest swamp phases, and suggest reduced effective precipitation during drought phases B and C (Figure 9). Drought phase A may have caused sufficient drying in the open water phase to stimulate productivity in hitherto limnic conditions, leading to rapid terrestrialization and infilling with litter (driving the conversion from open water wetland to forest swamp). This is consistent with the increase in S3 C observed in the Rock-Eval pyrolysis data (Figure 8). Drought phase B potentially drove the conversion of the forest swamp into an ombrotrophic peat dome, again by stimulating productivity in a previously seasonally flooded landscape. The resumption of peat accumulation after drought phase C also adds further weight to the growing body of evidence for the resilience of peatland ecosystems to recover from severe disturbances (e.g., Morris, Baird, Young, & Swindles, 2015; Swindles, Lamentowicz et al., 2016; Swindles, Morris et al., 2016; Waddington et al., 2015). The shift to ombrotrophic peat dome at ca. 3.9 ka BP is contemporaneous with the increased El Niño-Southern Oscillation

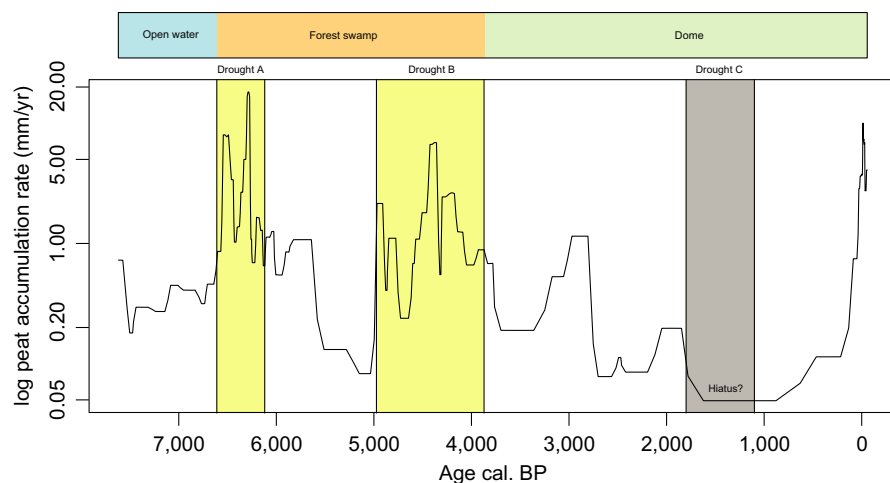


FIGURE 10 Peat accumulation rate (mm/year) plotted on a (natural) logarithmic scale with the three drought events and developmental phases illustrated [Colour figure can be viewed at wileyonlinelibrary.com]

(ENSO) activity identified from ~4.0 ka BP (Haug, Hughen, Sigman, Peterson, & Röhl, 2001; van Breukelen, Vonhof, Hellstrom, Wester, & Kroon, 2008), which may suggest climate variability played a role in stimulating the ecosystem state shift, alongside any autogenic mechanisms.

Gloor et al. (2013) suggested that there has been intensification of the Amazonian hydrological cycle over the last two decades and a marked increase in precipitation in north-western Amazonia (up to 80 mm/month from the period 1980–1990 to 2000–2009). Climate re-analysis data also show that there has been a recent shift to higher temperatures and increased precipitation at Aucayacu across all seasons (Fig. S12). The recent increase in wetness shown in our testate amoeba record (Figure 9) is consistent with a progressively wetter climate, although the effects of better test preservation in the uppermost peat cannot be discounted. The CMIP5 climate model ensemble projects that this region will continue to warm over the next ~80 years, with the wet season in particular becoming wetter (Fig. S12). Held and Soden (1995) and Wang et al. (2017) also suggested that rainfall in the Amazon lowlands is likely to increase, alongside the intensification of wet and dry phases (including more pronounced droughts).

4.2 | Implications and uncertainties

Our multiproxy dataset and conceptual model provide an important step in improving understanding of Amazonian peatland ecosystems. However, uncertainties remain over the relative controls of autogenic (e.g., peat growth and ecohydrology, plant succession) and allo-genic (e.g., climate, floodplain processes) controls on Amazonian peatland development. Mathematical models of peatland development (e.g., Baird, Morris, and Belyea (2012); Kurnianto et al., 2015; Morris et al., 2015; Swindles, Morris, Baird, Blaauw, & Plunkett, 2012) may prove useful tools for investigating the behaviour of Amazonian peatlands and the vulnerability of their C stores to climate change and human impacts. However, new data on the ecohydrological properties of these systems (e.g., plant communities, above and below-ground litter production and decomposition, and permeability) are needed for accurate parameterisation of these models. Detailed down-core studies of peat properties, C content, decomposition, palaeohydrology, and vegetation types, such as we present here, provide a crucial yardstick for testing model-based simulations of tropical peatland development.

A diversity of peatland types has been found in the PMFB (see Lähteenoja & Page, 2011). Future work should focus on understanding the developmental history of these different peatland types and whether there are developmental or successional pathways between them. Amazonian peatlands are important in terms of biodiversity, ecosystem services, and C storage, and they represent important archives of past climatic, ecological, and other environmental information (e.g., volcanic ash). Several infrastructure projects are planned in the PMFB including a proposal for constructing an electricity transmission line and service track through the Aucayacu peatland (Dourojeanni, 2016; Roucoux et al., 2017). We contend that policies

should focus on the conservation and protection of these vulnerable ecosystems.

5 | CONCLUSIONS

1. A multiproxy palaeoecological dataset shows that the oldest peat dome yet discovered in Amazonia developed in three distinct phases: (i) peat initiated in an abandoned river channel or back-water with standing open water and aquatic plants; (ii) inundated forest swamp; and (iii) raised peat dome (after ca. 3.9 ka BP). The presence of charcoal in the core shows that these ecosystems have been affected by fire on at least three occasions in the last 4,500 years.
2. Two phases of rapid carbon accumulation (ca. 6.6–6.1 and ca. 4.9–3.9 ka BP) potentially resulting from increased net primary productivity were seemingly driven by drier conditions during widespread drought events. A switch to ombrotrophy occurred after the ca. 4.5–4.2 ka BP drought phase suggesting a possible climatic control on tropical peatland developmental trajectories and ecosystem state shifts. A third drought phase at ca. 1.8–1.1 ka BP led to a collapse in carbon accumulation (potentially a hiatus), relating to increased decomposition from deeper water tables and/or lower net primary productivity during the ombrotrophic peat dome phase.
3. Our results suggest that future droughts will lead to phases of rapid carbon accumulation in some inundated tropical peat swamps, although this can lead ultimately to a shift to ombrotrophy and a subsequent return to lower carbon accumulation rates. Conversely, drought phases may lead to a collapse in carbon accumulation in ombrotrophic peat domes.
4. Amazonian peatlands are important in terms of biodiversity and carbon storage, and represent important archives of palaeoenvironmental information. Policies should focus on the conservation of these ecosystems.

ACKNOWLEDGEMENTS

This work was funded by a Royal Society research grant to GTS (grant no. 481831). GTS also acknowledges NERC Radiocarbon Analysis Allocation 1800.0414. DJC and AGS acknowledge the MILLI-PEAT project grant from NERC (NE/I012915/1) and NERC Radiocarbon Analysis Allocation 1681.1012. RFI is funded by NERC grant NE/K008536/1. We thank Ricardo Farroñay Peramas, Dennis del Castillo Torres, and Eurídice Honorio Coronado of the Instituto de Investigaciones de la Amazonía Peruana in Iquitos for assisting with fieldwork planning and logistics. Freddie Draper, Tom Kelly, and Tim Baker (University of Leeds) are thanked for useful discussions about Amazonian peatlands. We thank Andy Baird (University of Leeds) for commenting on the manuscript and providing insights into the controls on peat accumulation in tropical peatlands. Aristidis Vasques is acknowledged for piloting the boats and helping us run the

field campaign. Many thanks to Chris Williams (formerly University of Leeds) for assistance in the field. We acknowledge Lucho Freyre and David Huayaban (villagers from nearby Bellavista and Malvinas) for their assistance in the field and keeping us safe from Aucayacu's many venomous snakes.

ORCID

Graeme T. Swindles  <http://orcid.org/0000-0001-8039-1790>

Paul J. Morris  <http://orcid.org/0000-0002-1145-1478>

Bronwen Whitney  <http://orcid.org/0000-0002-2329-9645>

Mark W. Smith  <http://orcid.org/0000-0003-4361-9527>

REFERENCES

- Albrecht R., Sebag D., & Verrecchia E. (2015) Organic matter decomposition: Bridging the gap between Rock-Eval pyrolysis and chemical characterization (CPMAS ^{13}C NMR). *Biogeochemistry*, 122(1), 101–111.
- Ali, A. A., Ghaleb, B., Garneau, M., Asnong, H., & Loisel, J. (2008). Recent peat accumulation rates in minerotrophic peatlands of the Bay James region, Eastern Canada, inferred by ^{210}Pb and ^{137}Cs radiometric techniques. *Applied Radiation and Isotopes*, 66(10), 1350–1358. <https://doi.org/10.1016/j.apradiso.2008.02.091>
- Appleby, P. G. (2001). Chronostratigraphic techniques in recent sediments. In W. M. Last & J. P. Smol (Eds.), *Tracking environmental change using lake sediments: Basin analysis, coring, and chronological techniques* (pp. 171–203). Dordrecht, the Netherlands: Springer Netherlands.
- Baird, A. J., Low, R., Young, D., Swindles, G. T., Lopez, O. R., & Page, S. (2017). High permeability explains the vulnerability of the carbon store in drained tropical peatlands. *Geophysical Research Letters*, 44(3), 1333–1339. <https://doi.org/10.1002/2016GL072245>
- Baird, A. J., Milner, A. M., Blundell, A., Swindles, G. T., & Morris, P. J. (2016). Microform-scale variations in peatland permeability and their ecohydrological implications. *Journal of Ecology*, 104(2), 531–544. <https://doi.org/10.1111/1365-2745.12530>
- Baird, A. J., Morris, P. J., & Belyea, L. R. (2012). The DigiBog peatland development model 1: Rationale, conceptual model, and hydrological basis. *Ecohydrology*, 5(3), 242–255. <https://doi.org/10.1002/eco.230>
- Baker, P. A., Fritz, S. C., Garland, J., & Ekdahl, E. (2005). Holocene hydrologic variation at Lake Titicaca, Bolivia/Peru, and its relationship to North Atlantic climate variation. *Journal of Quaternary Science*, 20(7–8), 655–662. <https://doi.org/10.1002/jqs.987>
- Belyea, L. R., & Baird, A. J. (2006). Beyond “The limits to peat bog growth”: Cross-scale feedback in peatland development. *Ecological Monographs*, 76, 299–322. [https://doi.org/10.1890/0012-9615\(2006\)076\[0299:BTLTPB\]2.0.CO;2](https://doi.org/10.1890/0012-9615(2006)076[0299:BTLTPB]2.0.CO;2)
- Bennett, K. D. (1996). Determination of the number of zones in a biostratigraphical sequence. *New Phytologist*, 132(1), 155–170. <https://doi.org/10.1111/j.1469-8137.1996.tb04521.x>
- Bird, B. W., Abbott, M. B., Rodbell, D. T., & Vuille, M. (2011). Holocene tropical South American hydroclimate revealed from a decadal resolved lake sediment $\delta^{18}\text{O}$ record. *Earth and Planetary Science Letters*, 310(3–4), 192–202. <https://doi.org/10.1016/j.epsl.2011.08.040>
- Blaauw, M., & Christen, J. A. (2011). Flexible paleoclimate age-depth models using an autoregressive gamma process. *Bayesian Analysis*, 6(3), 457–474. <https://doi.org/10.1214/ba/1339616472>
- Bond, G., Showers, W., Cheseby, M., Lotti, R., Almasi, P., deMenocal, P., ... Bonani, G. (1997). A pervasive millennial-scale cycle in north atlantic holocene and glacial climates. *Science*, 278(5341), 1257–1266.
- Bond, G., Kromer, B., Beer, J., Muscheler, R., Evans, M. N., & Showers, W., ... Bonani, G. (2001). Persistent solar influence on North Atlantic climate during the Holocene. *Science*, 294(5549), 2130–2136. <http://science.sciencemag.org/content/294/5549/2130> <https://doi.org/10.1126/science.1065680>
- Booth, R. K., Jackson, S. T., Forman, S. L., Kutzbach, J. E., Bettis, E. A., Kreig, J., & Wright, D. K. (2005). A severe centennial-scale drought in midcontinental North America 4200 years ago and apparent global linkages. *The Holocene*, 15(3), 321–328. <https://doi.org/10.1191/0959683605hl825ft>
- Brienen, R. J. W., Phillips, O. L., Feldpausch, T. R., Gloor, E., Baker, T. R., & Lloyd, J., ... Zagt, R. J. (2015). Long-term decline of the Amazon carbon sink. *Nature*, 519(7543), 344–348. <https://doi.org/10.1038/nature14283>
- Burn, M. J., Mayle, F. E., & Killeen, T. J. (2010). Pollen-based differentiation of Amazonian rainforest communities and implications for lowland palaeoecology in tropical South America. *Palaeogeography, Palaeoclimatology, Palaeoecology*, 295(1–2), 1–18. <https://doi.org/10.1016/j.palaeo.2010.05.009>
- Bush, M. B., Silman, M. R., & Listopad, C. M. C. S. (2007). A regional study of Holocene climate change and human occupation in Peruvian Amazonia. *Journal of Biogeography*, 34(8), 1342–1356. <https://doi.org/10.1111/j.1365-2699.2007.01704.x>
- Carrie, J., Sanei, H., & Stern, G. (2012). Standardisation of Rock-Eval pyrolysis for the analysis of recent sediments and soils. *Organic Geochemistry*, 46, 38–53. <https://doi.org/10.1016/j.orggeochem.2012.01.011>
- Chambers, F. M., Beilman, D. W., & Yu, Z. (2011). Methods for determining peat humification and for quantifying peat bulk density, organic matter and carbon content for palaeostudies of climate and peatland carbon dynamics. *Mires and Peat*, 7, 1–10. http://pixelrauschen.de/wbmp/media/map07/map_07_07.pdf
- Correa-Metrio, A., Cabrera, K. R., & Bush, M. B. (2010). Quantifying ecological change through discriminant analysis: A paleoecological example from the Peruvian Amazon. *Journal of Vegetation Science*, 21(4), 695–704. <https://doi.org/10.1111/j.1654-1103.2010.01178.x>
- Davis, M. E., & Thompson, L. G. (2006). An Andean ice-core record of a middle Holocene mega-drought in north Africa and Asia. *Annals of Glaciology*, 43, 34–41. <http://research.bpcrc.osu.edu/lccore/publications/Annals%202006%20Davis%20%26%20LGT.pdf> <https://doi.org/10.3189/172756406781812456>
- De Vleeschouwer, F., Chambers, F. M., & Swindles, G. T. (2010). Coring and sub-sampling of peatlands for palaeoenvironmental research. *Mires and Peat*, 7(11), 1–10. http://pixelrauschen.de/wbmp/media/map07/map_07_01.pdf
- Debusk, W. F., & Reddy, K. R. (2005). Litter decomposition and nutrient dynamics in a phosphorus enriched everglades marsh. *Biogeochemistry*, 75(2), 217–240. <https://doi.org/10.1007/s10533-004-7113-0>
- Dietze, M., & Dietze, E. (2013) *EMMAgeo: End-Member Modelling of Grain-Size Data*. R package. Retrieved from <https://cran.r-project.org/web/packages/EMMAgeo/index.html>
- Dietze, E., Hartmann, K., Diekmann, B., Ijmker, J., Lehmkuhl, F., Opitz, S., ... Borchers, A. (2012). An end-member algorithm for deciphering modern detrital processes from lake sediments of Lake Donggi Cona, NE Tibetan Plateau, China. *Sedimentary Geology*, 243–244, 169–180. <https://doi.org/10.1016/j.sedgeo.2011.09.014>
- Dietze, E., Maussion, F., Ahlborn, M., Diekmann, B., Hartmann, K., & Henkel, K., ... Haberzettl, T. (2014). Sediment transport processes across the Tibetan Plateau inferred from robust grain-size end members in lake sediments. *Climate of the Past*, 10(1), 91–106. <https://doi.org/10.5194/cp-10-91-2014>
- Dommain, R., Cobb, A. R., Joosten, H., Glaser, P. H., Chua, A. F. L., & Gandois, L., ... Harvey, C. F. (2015). Forest dynamics and tip-up

- pools drive pulses of high carbon accumulation rates in a tropical peat dome in Borneo (Southeast Asia). *Journal of Geophysical Research: Biogeosciences*, 120(4), 617–640. <https://doi.org/10.1002/2014jg002796>
- Doughty, C. E., Metcalfe, D. B., Girardin, C. A. J., Amézquita, F. F., Cabrera, D. G., & Huasco, W. H., ... Malhi, Y. (2015). Drought impact on forest carbon dynamics and fluxes in Amazonia. *Nature*, 519(7541), 78–82. <https://doi.org/10.1038/nature14213>
- Dourojeanni, M. J. (2016). *Revisando temas actuales e importantes de la Amazonía peruana*. SPDA Actualidad Ambiental. Retrieved from <http://www.actualidadambiental.pe/?p=41462>. Accessed March 2017.
- Draper, F. C., Roucoux, K. H., Lawson, I. T., A Mitchard, E. T., Honorio Coronado, E. N., & Låhteenoja, O., ... Baker, T. R. (2014). The distribution and amount of carbon in the largest peatland complex in Amazonia. *Environmental Research Letters*, 9(12), 124017. <https://doi.org/10.1088/1748-9326/9/12/124017>
- Fægri, K., & Iversen, J. (1989). *Textbook of pollen analysis* (4th ed.). Chichester, UK and New York, NY: John Wiley.
- Fauset, S., Johnson, M. O., Gloor, M., Baker, T. R., Monteagudo M, A., & Brienen, R. J. W., ... Phillips, O. L. (2015). Hyperdominance in Amazonian forest carbon cycling. *Nature Communications*, 6, 6857. <https://doi.org/10.1038/ncomms7857>
- Feldpausch, T. R., Phillips, O. L., Brienen, R. J. W., Gloor, E., Lloyd, J., & Lopez-Gonzalez, G., ... Vos, V. A. (2016). Amazon forest response to repeated droughts. *Global Biogeochemical Cycles*, 30(7), 964–982. <https://doi.org/10.1002/2015GB005133>
- Flantua, S. G. A., Hooghiemstra, H., Vuille, M., Behling, H., Carson, J. F., & Gosling, W. D., ... González-Arango, C. (2016). Climate variability and human impact in South America during the last 2000 years: Synthesis and perspectives from pollen records. *Climate of the Past*, 12(2), 483–523. <https://doi.org/10.5194/cp-12-483-2016>
- Foster, D. R., & Wright, H. E. (1990). Role of ecosystem development and climate change in bog formation in Central Sweden. *Ecology*, 71, 450–463. <https://doi.org/10.2307/1940300>
- Gałka, M., Miotk-Szpiganowicz, G., Goslar, T., Jeśko, M., van der Knaap, W. O., & Lamentowicz, M. (2013). Palaeohydrology, fires and vegetation succession in the southern Baltic during the last 7500 years reconstructed from a raised bog based on multi-proxy data. *Palaeogeography, Palaeoclimatology, Palaeoecology*, 370, 209–221. <https://doi.org/10.1016/j.palaeo.2012.12.011>
- Glaser, P. H., Hansen, B. C. S., Siegel, D. I., Reeve, A. S., & Morin, P. J. (2004). Rates, pathways and drivers for peatland development in the Hudson Bay Lowlands, northern Ontario, Canada. *Journal of Ecology*, 92, 1036–1053. <https://doi.org/10.1111/j.0022-0477.2004.00931.x>
- Gloor, M., Brienen, R. J. W., Galbraith, D., Feldpausch, T. R., Schöngart, J., & Guyot, J.-L., ... Phillips, O. L. (2013). Intensification of the Amazon hydrological cycle over the last two decades. *Geophysical Research Letters*, 40(9), 1729–1733. <https://doi.org/10.1002/grl.50377>
- Hammer, R., Harper, D. A. T., & Ryan, P. D. (2001). PAST: Paleontological statistics software package for education and data analysis. *Palaeontologia Electronica*, 4, 9. http://palaeo-electronica.org/2001_1/past/issue1_01.htm
- Haug G. H., Hughen K. A., Sigman D. M., Peterson L. C., & Röhl U. (2001). Southward migration of the intertropical convergence zone through the Holocene. *Science*, 293(5533), 1304–1308.
- Held, I. M., & Soden, B. J. (1995). Robust responses of the hydrologic cycle to global warming. *Journal of Climate*, 19, 5686–5699. <https://doi.org/10.1175/JCLI3990.1>
- Hirano, T., Segah, H., Kusin, K., Limin, S., Takahashi, H., & Osaki, M. (2012). Effects of disturbances on the carbon balance of tropical peat swamp forests. *Global Change Biology*, 18(11), 3410–3422. <https://doi.org/10.1111/j.1365-2486.2012.02793.x>
- Hooijer, A., Page, S., Canadell, J. G., Silvius, M., Kwadijk, J., Wösten, H., & Jauhiainen, J. (2010). Current and future CO₂ emissions from drained peatlands in Southeast Asia. *Biogeosciences*, 7(5), 1505–1514. <https://doi.org/10.5194/bg-7-1505-2010>
- Jowsey, P. C. (1966). An improved peat sampler. *New Phytologist*, 65, 245–248. <https://doi.org/10.1111/nph.1966.65.issue-2>
- Juggins, S. (2015). *Rioja: Analysis of Quaternary Science Data*. R package. Retrieved from <http://cran.r-project.org/package=rioja>
- Junk, W. J. (1989). Flood tolerance and tree distribution in central Amazonian floodplains. In L. B. Holm-Nielsen, H. Nielson & H. Balsev (Eds.), *Tropical forests: Botanical dynamics, speciation and diversity* (pp. 47–64). London: Academic Press. <https://doi.org/10.1016/B978-0-12-353550-4.50012-5>
- Kahn, F., & Mejia, K. (1990). Palm communities in wetland forest ecosystems of Peruvian Amazonia. *Forest Ecology and Management*, 33–34, 169–179. [https://doi.org/10.1016/0378-1127\(90\)90191-D](https://doi.org/10.1016/0378-1127(90)90191-D)
- Kelly, T. J., Lawson, I. T., Roucoux, K. H., Baker, T. R., Jones, T. D., & Sanderson, N. K. (2017). The vegetation history of an Amazonian domed peatland. *Palaeogeography, Palaeoclimatology, Palaeoecology*, 468, 129–141. <https://doi.org/10.1016/j.palaeo.2016.11.039>
- Klovan, J. E., & Imbrie, J. (1971). An algorithm and FORTRAN-IV program for large-scale Q-mode factor analysis and calculation of factor scores. *Journal of the International Association for Mathematical Geology*, 3, 61–77. <https://doi.org/10.1007/BF02047433>
- Kurnianto, S., Warren, M., Talbot, J., Kauffman, B., Murdiyarto, D., & Frohling, S. (2015). Carbon accumulation of tropical peatlands over millennia: A modeling approach. *Global Change Biology*, 21(1), 431–444. <https://doi.org/10.1111/gcb.12672>
- Lafargue, E., Espitalité, J., Marquis, F., & Pillot, D. (1998). Rock-Eval™ 6 applications in hydrocarbon exploration, production and soil contamination studies. *Revue de L'Institut Français de Pétrole [Review of the French Petroleum Institute]*, 53(4), 421–437. <https://doi.org/10.2516/ogst:1998036>
- Låhteenoja, O., & Page, S. (2011). High diversity of tropical peatland ecosystem types in the Pastaza-Marañón basin, Peruvian Amazonia. *Journal of Geophysical Research: Biogeosciences*, 116(2), G02025. <https://doi.org/10.1029/2010JG001508>
- Låhteenoja, O., Reátegui, Y. R., Räsänen, M., Torres, D. D. C., Oinonen, M., & Page, S. (2012). The large Amazonian peatland carbon sink in the subsiding Pastaza-Marañón foreland basin. *Peru. Global Change Biology*, 18(1), 164–178. <https://doi.org/10.1111/j.1365-2486.2011.02504.x>
- Låhteenoja, O., Ruokolainen, K., Schulman, L., & Alvarez, J. (2009). Amazonian floodplains harbour minerotrophic and ombrotrophic peatlands. *Catena*, 79(2), 140–145. <https://doi.org/10.1016/j.catena.2009.06.006>
- Låhteenoja, O., Ruokolainen, K., Schulman, L., & Oinonen, M. (2009). Amazonian peatlands: An ignored C sink and potential source. *Global Change Biology*, 15(9), 2311–2320. <https://doi.org/10.1111/j.1365-2486.2009.01920.x>
- Ledru, M.-P. (2001). Late Holocene rainforest disturbance in French Guiana. *Review of Palaeobotany and Palynology*, 115, 161–170. [https://doi.org/10.1016/S0034-6667\(01\)00068-9](https://doi.org/10.1016/S0034-6667(01)00068-9)
- Lehner, B., Verdin, K., & Jarvis, A. (2006). *HydroSHEDS technical documentation*. Washington, DC: World Wildlife Fund US. <http://hydrosheds.cr.usgs.gov>
- Lopez, O. R., & Kursar, T. A. (2003). Does flood tolerance explain tree species distribution in tropical seasonally flooded habitats? *Oecologia*, 136, 193–204. <https://doi.org/10.1007/s00442-003-1259-7>
- Malhi, Y., Wood, D., Baker, T. R., Wright, J., Phillips, O. L., & Cochrane, T., ... Vinceti, B. (2006). The regional variation of aboveground live biomass in old-growth Amazonian forests. *Global Change Biology*, 12(7), 1107–1138. <https://doi.org/10.1111/j.1365-2486.2006.01120.x>
- Martinez, R., Ruiz, D., Andrade, M., Blacutt, L., Pabon, D., Jaimes, E., ... Jorgensen, P. M. (2011). Synthesis of the climate of the tropical Andes. In: S. K. Herzog, R. Martinez & H. Tiessen (Eds.), *Climate change and biodiversity in the tropical Andes* (pp. 97–109). Sao Jose

- dos Campos, Brazil, Paris, France: MacArthur Foundation, Inter-American Institute of Global Change Research (IAI) and Scientific Committee on Problems of the Environment (SCOPE), vol 348. ISBN: 978-85-99875-05-627.
- Mayle, F. E., & Power, M. J. (2008). Impact of a drier Early–Mid-Holocene climate upon Amazonian forests. *Philosophical Transactions of the Royal Society of London B: Biological Sciences*, 363(1498), 1829–1838. <https://doi.org/10.1098/rstb.2007.0019>
- McMichael, C. H., Correa-Metrio, A., & Bush, M. B. (2012). Pre-Columbian fire regimes in lowland tropical rainforests of southeastern Peru. *Palaeogeography, Palaeoclimatology, Palaeoecology*, 342, 73–83. <https://doi.org/10.1016/j.palaeo.2012.05.004>
- Met Office (2011). *Climate: Observations, projections and impacts: Peru*. Exeter, UK: Met Office.
- Meyers, P. A., & Ishiwatari, R. (1993). The early diagenesis of organic matter in lacustrine sediments. In M. H. Engel & S. A. Macko (Eds.), *Organic geochemistry: Principles and applications* (pp. 185–209). Boston, MA: Springer US. <https://doi.org/10.1007/978-1-4615-2890-6>
- Moore, S., Evans, C. D., Page, S. E., Garnett, M. H., Jones, T. G., & Freeman, C., ... Gaudi, V. (2013). Deep instability of deforested tropical peatlands revealed by fluvial organic carbon fluxes. *Nature*, 493(7434), 660–663. <https://doi.org/10.1038/nature11818> <https://doi.org/10.1038/nature11818>
- Morris, P. J., Baird, A. J., Young, D. M., & Swindles, G. T. (2015). Untangling climate signals from autogenic changes in long-term peatland development. *Geophysical Research Letters*, 42(24), 10788–10797. <https://doi.org/10.1002/2015GL066824>
- Murray, M. R. (2002). Is laser particle size determination possible for carbonate-rich lake sediments? *Journal of Paleolimnology*, 27, 173–183. <https://doi.org/10.1023/A:1014281412035>
- Nebel, G., Kvist, L. P., Vanclay, J. K., Christensen, H., Freitas, L., & Ruiz, J. (2001). Structure and floristic composition of flood plain forests in the Peruvian Amazon: I. Overstorey. *Forest Ecology and Management*, 150, 27–57. [https://doi.org/10.1016/S0378-1127\(00\)00680-0](https://doi.org/10.1016/S0378-1127(00)00680-0)
- Oksanen, J., Blanchet, F., Friendly, M., Kindt, G. R., Legendre, P., & McGlenn, D., ... Wagner, H. (2013). *Vegan: Community Ecology Package*. R package. Retrieved from <http://cran.r-project.org/package=vegan>.
- Page, S. E., Rieley, J. O., & Banks, C. J. (2011). Global and regional importance of the tropical peatland carbon pool. *Global Change Biology*, 17(2), 798–818. <https://doi.org/10.1111/j.1365-2486.2010.02279.x>
- Piperno, D. R., & Becker, P. (1996). Vegetational history of a site in the central Amazon Basin derived from phytolith and charcoal records from natural soils. *Quaternary Research*, 45(2), 202–209. <https://doi.org/10.1006/qres.1996.0020>
- Pratte, S., Mucci, A., & Garneau, M. (2013). Historical records of atmospheric metal deposition along the St. Lawrence Valley (eastern Canada) based on peat bog cores. *Atmospheric Environment*, 79, 831–840. <https://doi.org/10.1016/j.atmosenv.2013.07.063>
- R Core Team (2016). *R: A language and environment for statistical computing*. Vienna, Austria: R Foundation for Statistical Computing. <https://www.R-project.org/>
- Räsänen, M. E., Salo, J. S., Jungnert, H., & Pittman, L. R. (1990). Evolution of the western Amazon lowland relief: Impact of Andean foreland dynamics. *Terra Nova*, 2, 320–332. <https://doi.org/10.1111/j.1365-3121.1990.tb00084.x>
- Reczuga, M. K., Swindles, G. T., Grewling, Ł., & Lamentowicz, M. (2015). *Arcella peruviana* sp. nov. (Amoebozoa: Arcellinida, Arcellidae), a new species from a tropical peatland in Amazonia. *European Journal of Protistology*, 51(5), 437–449. <https://doi.org/10.1016/j.ejop.2015.01.002>
- Reimer, P. J., Bard, E., Bayliss, A., Beck, J. W., Blackwell, P. G., & Ramsey, C. B., ... van der Plicht, J. (2013). IntCal13 and Marine13 radiocarbon age calibration curves 0–50,000 years cal BP. *Radiocarbon*, 55(4), 1869–1887. https://doi.org/10.2458/azu_js_rc.55.16947
- Roland, T. P., Caseldine, C. J., Charman, D. J., Turney, C. S. M., & Amesbury, M. J. (2014). Was there a ‘4.2 ka event’ in Great Britain and Ireland? Evidence from the peatland record. *Quaternary Science Reviews*, 83, 11–27. <https://doi.org/10.1016/j.quascirev.2013.10.024>
- Roos-Barraclough, F., van der Knaap, W. O., van Leeuwen, J. F. N., & Shoty, W. (2004). A late-glacial and Holocene record of climatic change from a Swiss peat humification profile. *The Holocene*, 14, 7–19. <https://doi.org/10.1191/0959683604hl685rp>
- Roucoux, K. H., Lawson, I. T., Baker, T. R., Del Castillo Torres, D., Draper, F. C., & Lähteenoja, O., ... Vriesendorp, C. (2017). Threats to intact tropical peatlands and opportunities for their conservation. *Conservation Biology*. in press. <https://doi.org/10.1111/cobi.12925>
- Roucoux, K. H., Lawson, I. T., Jones, T. D., Baker, T. R., Coronado, E. N. H., Gosling, W. D., & Lähteenoja, O. (2013). Vegetation development in an Amazonian peatland. *Palaeogeography, Palaeoclimatology, Palaeoecology*, 374, 242–255. <https://doi.org/10.1016/j.palaeo.2013.01.023>
- Rydin, H., & Jeglum, J. K. (2006). *The biology of peatlands* (p. 343). Oxford: Oxford University Press. <https://doi.org/10.1093/acprof:oso/9780198528722.001.0001>
- Sanei, H., Stasiuk, L. D., & Goodarzi, F. (2005). Petrological changes occurring in organic matter from recent lacustrine sediments during thermal alteration by Rock-Eval pyrolysis. *Organic Geochemistry*, 36(8), 1190–1203. <https://doi.org/10.1016/j.orggeochem.2005.02.009>
- Swindles, G. T., Holden, J., Raby, C. L., Turner, T. E., Blundell, A., & Charman, D. J., ... Kløve, B. (2015). Testing peatland water-table depth transfer functions using high-resolution hydrological monitoring data. *Quaternary Science Reviews*, 120, 107–117. <https://doi.org/10.1016/j.quascirev.2015.04.019>
- Swindles, G. T., Lamentowicz, M., Reczuga, M., & Galloway, J. M. (2016). Palaeoecology of testate amoebae in a tropical peatland. *European Journal of Protistology*, 55, 181–189. <https://doi.org/10.1016/j.ejop.2015.10.002>
- Swindles, G. T., Morris, P. J., Baird, A. J., Blaauw, M., & Plunkett, G. (2012). Ecohydrological feedbacks confound peat-based climate reconstructions. *Geophysical Research Letters*, 39, L11401. <https://doi.org/10.1029/2012GL051500>
- Swindles, G. T., Morris, P. J., Wheeler, J., Smith, M. W., Bacon, K. L., & Edward Turner, T., ... Galloway, J. M. (2016). Resilience of peatland ecosystem services over millennial timescales: Evidence from a degraded British bog. *Journal of Ecology*, 104(3), 621–636. <https://doi.org/10.1111/1365-2745.12565>
- Swindles, G. T., Reczuga, M., Lamentowicz, M., Raby, C. L., Turner, T. E., & Charman, D. J., ... Mullan, D. J. (2014). Ecology of testate amoebae in an Amazonian peatland and development of a transfer function for palaeohydrological reconstruction. *Microbial Ecology*, 68(2), 284–298. <https://doi.org/10.1007/s00248-014-0378-5>
- Tolonen, K., & Turunen, J. (1996). Accumulation rates of carbon in mires in Finland and implications for climate change. *The Holocene*, 6(2), 171–178. <https://doi.org/10.1177/095968369600600204>
- Troels-Smith, J. (1955). Karakterisering af løse jordarter. Characterization of unconsolidated sediments. *Danmarks Geologiske Undersøgelse Serier*, IV(3), 1–73.
- van Breukelen, M. R., Vonhof, H. B., Hellstrom, J. C., Wester, W. C. G., & Kroon, D. (2008). Fossil dripwater in stalagmites reveals Holocene temperature and rainfall variation in Amazonia. *Earth and Planetary Science Letters*, 275(1–2), 54–60. <https://doi.org/10.1016/j.epsl.2008.07.060>
- van Hengstum, P. J., Reinhardt, E. G., Boyce, J. I., & Clark, C. (2007). Changing sedimentation patterns due to historical land-use change in Frenchman’s Bay, Pickering, Canada: Evidence from high-resolution textural analysis. *Journal of Paleolimnology*, 37(4), 603–618. <https://doi.org/10.1007/s10933-006-9057-y>
- Waddington, J. M., Morris, P. J., Kettridge, N., Granath, G., Thompson, D. K., & Moore, P. A. (2015). Hydrological feedbacks in northern peatlands. *Ecohydrology*, 8(1), 113–127. <https://doi.org/10.1002/eco.1493>
- Wang, X., Edwards, R. L., Auler, A. S., Cheng, H., Kong, X., & Wang, Y., ... Chiang, H.-W. (2017). Hydroclimate changes across the Amazon

- lowlands over the past 45,000 years. *Nature*, 541(7636), 204–207. <https://doi.org/10.1038/nature20787>
- Watson, E. J., Swindles, G. T., Savov, I. P., & Bacon, K. L. (2015). First discovery of Holocene cryptotephra in Amazonia. *Scientific Reports*, 5, 15579. <https://doi.org/10.1038/srep15579>
- Weltje, G. J. (1997). End-member modeling of compositional data: Numerical-statistical algorithms for solving the explicit mixing problem. *Mathematical Geology*, 29, 503–549. <https://doi.org/10.1007/BF02775085>
- Weng, C., Bush, M. B., & Athens, J. S. (2002). Holocene climate change and hydrarch succession in lowland Amazonian Ecuador. *Review of Palaeobotany and Palynology*, 120(1–2), 73–90. [https://doi.org/10.1016/S0034-6667\(01\)00148-8](https://doi.org/10.1016/S0034-6667(01)00148-8)
- Worbes, M. (1997). The forest ecosystem of the floodplains. In W. J. Junk (Ed.), *The central Amazon floodplain: Ecology of a pulsing system* (pp. 223–265). Berlin, Heidelberg, Germany: Springer Berlin Heidelberg. <https://doi.org/10.1007/978-3-662-03416-3>
- Yeloff, D., & Mauquoy, D. (2006). The influence of vegetation composition on peat humification: Implications for palaeoclimatic studies. *Boreas*, 35, 662–673. <https://doi.org/10.1111/bor.2006.35.issue-4>

SUPPORTING INFORMATION

Additional Supporting Information may be found online in the supporting information tab for this article.

How to cite this article: Swindles GT, Morris PJ, Whitney B, et al. Ecosystem state shifts during long-term development of an Amazonian peatland. *Glob Change Biol.* 2018;24:738–757. <https://doi.org/10.1111/gcb.13950>